Physics – Uspekhi **53** (6) 537 – 560 (2010)

REVIEWS OF TOPICAL PROBLEMS PACS numbers: 61.44.Fw, 71.23.Ft, 75.50.Lk

Quasicrystals

Yu Kh Vekilov, M A Chernikov

DOI: 10.3367/UFNe.0180.201006a.0561

Contents

Abstract. We review the structure of quasicrystals and their electronic spectra, lattice excitation spectra, physical properties, and applications. The aperiodic filling of space according to certain rules with several structural units or overlapping atomic clusters is discussed. Perfect tiling, random tiling, and icosahedral glass models, as well as phason strain are considered. The effect that the aperiodic long-range order and local atomic structure have on electron and thermal transport and on the optical, magnetic, and other properties is examined.

1. Introduction

The lattice symmetry of periodically ordered crystals is due to the periodic arrangement of their atoms — that is, parallel transfers or translations through the length of the basis vectors of the lattice turn the lattice into itself. Unit cell translations through the basis vectors of the lattice ensure dense filling of the entire space without voids and overlaps and thereby construction of the crystal lattice. Besides translational symmetry, the crystal lattice may exhibit symmetry with respect to rotations and reflections. Translational symmetry imposes constraints on possible orders of symmetry axes in crystal lattices. Periodically ordered crystals may have 2-, 3-, 4-, and 6-fold rotational symmetry axes. Rotations about symmetry axes of the fifth order or any one higher than the sixth fail to transform the lattice into itself; therefore, such symmetry axes are forbidden for crystals. The proof of this fundamental theorem of classical crystallography can be found, inter alia, in the *Course of Theoretical Physics*, Vol. 5 by L D Landau and E M Lifshitz [1].

As is well known, periodicity is not a necessary condition for the existence of long-range atomic order. For example, quasicrystals possess a strictly aperiodic long-range order of the quasiperiodic type. They lack the translational symmetry that constrains possible order of symmetry axes; therefore, they may also have symmetry axes of those orders that are forbidden for ordinary periodically ordered crystals, as illustrated by the example of 'Penrose tiling', i.e., a lattice model of the two-dimensional quasicrystal. To recall, the notion of the unit cell does not allow simple generalization over quasicrystals because quasicrystal lattices are necessarily built up of two or more types of structural blocks. Penrose tiling consists of two different structural blocks, narrow and wide rhombi with acute vertex angles of $\pi/5$ and $2\pi/5$, respectively. Laying of these two rhombi, starting from 5 broad ones that have a common vertex, in accordance with certain rules, results in a quasiperiodic covering of the plane without voids or overlaps. Penrose tiling has a single point rotation about which by an angle of $2\pi/5$ transforms the lattice into itself, which suggests an exact axis of 5-fold symmetry. Moreover, Penrose tiling exhibits rotational symmetry of the tenth order in the sense that rotation by an angle of $\pi/5$ leads to a lattice statistically indistinguishable from the initial one; such lattices are indiscernible, for

Yu Kh Vekilov National University of Science and Technology 'MISIS', Leninskii prosp. 4, 119049 Moscow, Russian Federation
Tel./Fax (7-495) 955 00 62
E-mail: yuri.vekilov@gmail.com
M A Chernikov Russian Research Centre 'Kurchatov Institute' pl. Kurchatova 1, 123182 Moscow, Russian Federation
Tel. (7-499) 196 99 35
Fax (7-499) 196 59 73
E-mail: mchernikov@earthlink.net
National University of Science and Technology 'MISIS' Leninskii prosp. 4, 119049 Moscow, Russian Federation

Received 1 July 2009, revised 16 November 2009
Uspekhi Fizicheskikh Nauk **180** (6) 561 – 586 (2010)
DOI: 10.3367/UFNr.0180.201006a.0561
Translated by Yu V Morozov; edited by A Radzig

example, in diffraction experiments. The quasicrystal lattice can also be constructed by analogy with laying the Penrose tiling in the three-dimensional case. An example is the icosahedrally symmetric Ammann–Mackay network, i.e., a space tightly filled (according to certain rules) with prolate and oblate rhombohedrons with definite vertex angles. Quasicrystal lattices are discussed at length in Section 2.

Aperiodic long-range atomic order with icosahedral symmetry was first discovered in 1984 by Shechtman, Blech, Gratias, and Cahn [2], who reported unusual electron diffraction patterns in a rapidly cooled $Al_{86}Mn_{14}$ alloy. To begin with, they observed long-range order of the noncrystalline type in the form of sharp Bragg peaks with the symmetry axis of the tenth order incompatible with periodic ordering. Second, the intensity of diffraction spots did not decrease with the distance from the center of the diffraction pattern, as in the case of periodically ordered crystals. Third, consideration of a sequence of reflections from the center of the diffraction pattern to its periphery showed that spacings between the reflections are related by powers of number $\tau = (\sqrt{5}+1)/2$ or the golden ratio (see Appendix 8.1). Fourth, $Al_{86}Mn_{14}$ diffraction patterns required six Miller indices to be described instead of the three necessary to label Bragg reflections in a periodically ordered crystal. Comprehensive analysis of diffraction patterns obtained by moving along different crystallographic directions revealed the occurrence of 6 symmetry axes of the fifth order, 10 symmetry axes of the third order, and 15 of the second order, allowing for the conclusion that the structure of the $Al_{86}Mn_{14}$ alloy has a point symmetry group $m\bar{3}\bar{5}$, i.e., an icosahedron symmetry group. Figure 1 shows electron diffraction patterns along symmetry axes of the second, third, and fifth orders of a typical icosahedral $Al_{69.5}Pd_{21}Mn_{9.5}$ alloy.

Theoretical justification for the existence of Bragg peaks in the diffraction patterns of a structure with icosahedral symmetry was provided by Levine and Steinhardt [3]. They constructed a quasicrystal model based on two unit cells with an irrational ratio of their number and showed that the diffraction pattern of aperiodic packing with icosahedral symmetry shows Bragg reflections on the dense set of sites in the reciprocal space with intensities consistent with those obtained for the $Al_{86}Mn_{14}$ alloy. A quasicrystalline structure can be produced by aperiodic filling of the space with a few structural units with a corresponding motive (atomic decoration) in the absence of voids and overlaps. An equivalent method of construction of a quasicrystalline structure consists in aperiodic filling of the space with identical atomic clusters overlapping in accordance with certain rules (the quasicell method). It seems likely that the physical causes behind the formation of quasicrystalline structures should be sought in crystal chemistry which 'requires' icosahedral short-range order in the atomic packing and 'imposes' on the medium preferred symmetry axes of the 5th order in the direction of chemical bonds; these requirements are incompatible with translational long-range order. Monoelement quasicrystals are nonexistent. Quasicrystalline structures occur in metal alloys, with real quasicrystals frequently representing imperfect, i.e., defective, realization of a perfect quasicrystalline structure in the ground state. The quasicrystalline structure is similar to other types of structures in terms of energy. Depending on the preparation conditions, composition, and thermal treatment, a quasicrystal may be found in the perfect quasicrystalline state even in the absence of characteristic static distortions (phasons) or in the microcrystalline state with a coherence length on the order of 10^2 Å and general pseudoicosahedral symmetry.

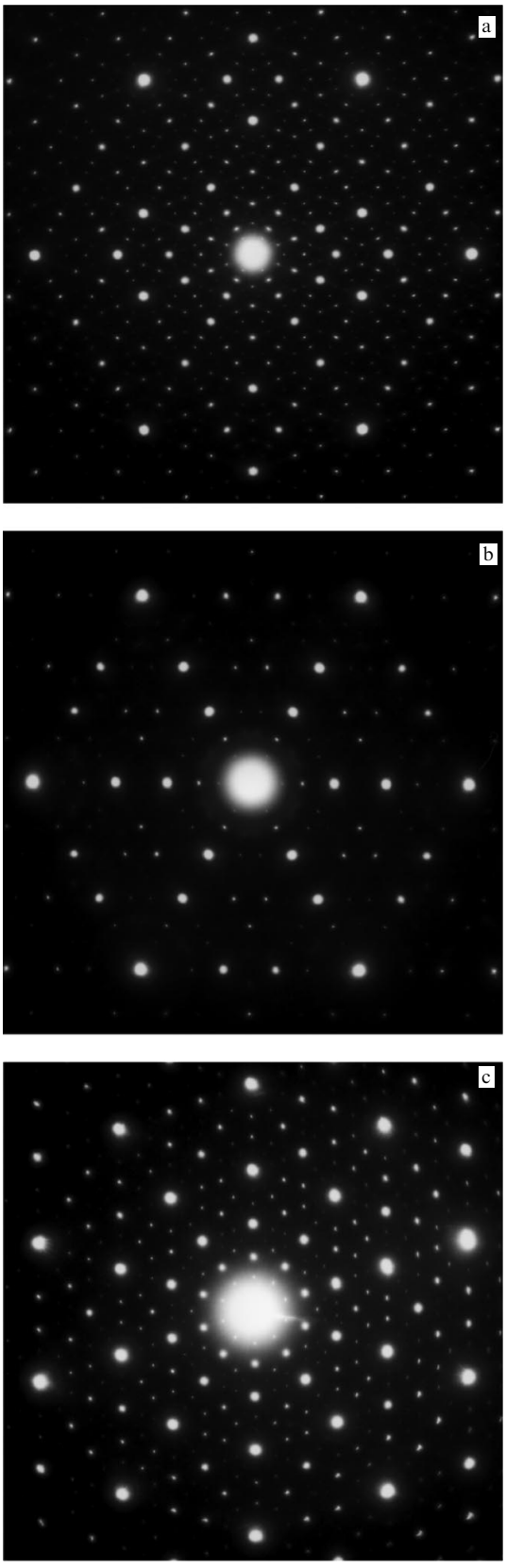

Figure 1. Electron diffraction patterns of the icosahedral $Al_{69.5}Pd_{21}Mn_{9.5}$ phase: (a) along the symmetry axis of the second order, (b) along the symmetry axis of the third order, and (c) along the symmetry axis of the fifth order (provided by K Edagawa).

Quasiperiodic structures were subjects of investigations in mathematics, physics, and materials science before the discovery of quasicrystals, as well. In the early 20th century, mathematicians showed interest in the aperiodic functions whose Fourier transform contains sharp peaks (e.g., function $f(x) = \cos qx + \cos Qx$, where the Q/q ratio is an irrational number). The concept of aperiodic mosaics has roots stretching back into antiquity and has been extensively studied since then in geometry [4]. The term 'aperiodic crystal' was introduced by Schrödinger [5] in connection with the discussion of gene structure. Before the discovery of quasicrystals, solid-state physics studied incommensurably modulated phases (see Appendix 8.2) and composite crystals with a modulated structure, whose diffraction patterns exhibited Bragg maxima arranged with usual crystal symmetry but surrounded by satellite reflections. Also, physicists were aware of the existence of icosahedral short-range order in complex metallic alloys, metallic glasses, boron compounds containing coupled B_{12} icosahedrons [6], the $(B_{12}H_{12})^{2-}$ anion [7], clusters of alkali and noble metals [8], and intermetallic compounds currently known as periodic approximants of quasicrystals. However, the necessity of periodicity for the emergence of long-range order was not questioned until issuing the report on the $Al_{86}Mn_{14}$ icosahedral phase with long-range atomic order [2]. A plethora of publications on the structure and properties of quasicrystals over subsequent years have made the physics of quasicrystals a self-contained branch of solid-state physics.

Quasicrystals could have been discovered earlier. Indeed, Bradley and Goldschmidt [9] studied slowly cooled ternary Al–Cu–Fe alloys by X-ray structural analysis as early as 1939 and reported the finding of a ternary compound with Al_6Cu_2Fe composition of unknown structure, which they called the ψ phase. In 1971, Prevarskii [10] investigated phase equilibriums in the Al–Cu–Fe system and showed that the ψ phase includes a small homogeneous region and is the sole triple phase in this ternary system at a temperature of 800 °C. In 1987, Tsai et al. [11] demonstrated that an alloy similar to the ψ phase in composition constitutes a thermodynamically stable icosahedral quasicrystal. In 1955, Hardy and Silcock [12] discovered the new phase (designated by them as T2 phase) in the Al–Cu–Li system, whose diffraction patterns defied indexing. Its composition resembled that of Al_6CuLi_3 and corresponded to the icosahedral phase of Al–Cu–Li [13]. In 1978, Sastry et al. [14] observed diffraction patterns with pseudopentagonal symmetry in the Al–Pd system [14]. Later on, a decagonal quasicrystalline phase was also discovered in this system. Finally, Padezhnova and coworkers [15] reported finding an R phase in Y–Mg–Zn system and the failure to interpret its X-ray powder diffraction pattern; in a later study, Luo et al. [16] showed that this phase had the icosahedral structure. None of these reports were given proper attention in due time, which set back the discovery of quasicrystals by many years.

It is noteworthy that quasicrystalline alloys contain atoms of transition, noble, and rare-earth metals; this fact is probably responsible for the crystal chemistry of the short-range atomic order. Many quasicrystalline phases exist in the equilibrium phase diagram in a relatively narrow concentration region. The equilibrium thermodynamic, transport, magnetic, and mechanical properties of quasicrystals, as well as their single-particle and collective excitation spectra, differ from those of the crystalline and amorphous phases of similar composition. Specific properties of quasicrystals are due to both the aperiodic long-range order and the local atomic structure. Being alloys of metallic elements, quasicrystals are neither ordinary metals nor insulators or semiconductors. Unlike insulators, quasicrystals have a nonzero density of electronic states at the Fermi level, $n(E_F)$, although it is lower than in typical metals. The characteristic features of quasicrystal electronic spectra include a pseudogap in the density of electronic state at the Fermi level and the fine peak structure $n(E)$ that influence the physical properties of quasicrystals.

A wealth of experimental and theoretical data on quasicrystal structure, properties, and methods of formation has been accumulated over the more than 20-year history of investigations; a number of ideas concerning their practical applications have been proposed and implemented. The voluminous body of quasicrystal literature comprises numerous articles, conference proceedings, and monographs (see, for instance, Refs [17–29]). The aim of this review is to present the main current concepts concerning the structure and physical properties of quasicrystals. It is intended for a wide circle of readers. No special emphasis is laid on concrete objects or the details of theoretical and experimental methods of analysis. Peculiarities of the structure and properties distinguishing quasicrystals from other solids are considered, and the possibilities of their practical applications and prospects for further studies are briefly discussed.

2. The structure of quasicrystals

2.1 Types of quasicrystals and methods for their formation

There are quasicrystals with orientational symmetries other than icosahedral. Axial quasicrystals having rotation symmetry axes of the 8th, 10th, and 12th orders were called octagonal, decagonal, and dodecagonal phases, respectively. They exhibit a quasiperiodic arrangement of atoms in the planes normal to the symmetry axes of the eighth, tenth, and twelfth orders. The quasiperiodic planes themselves are packed in a periodic manner. Figure 2 depicts electron diffraction patterns of the so-called basic decagonal phase of the Al–Ni–Co system with a high Co content for three directions of electron beam propagation in the sample, viz. along the decagonal axis and A2P- and A2D-axes, i.e., two different symmetry axes of the 2nd order [30]. Moreover, there occur alloys with unidirectional quasiperiodicity.

Al–Mn alloys and other quasicrystalline phases discovered soon after them proved to be metastable (they went to a periodically ordered state when heated). They could be prepared by rapid quenching of the melt or by other exotic methods [2, 31]. Metastable quasicrystals were characterized by a high degree of disorder that complicated evaluation of the possible effect of quasiperiodicity on their physical properties. Results obtained with samples of metastable phases indicated that the physical properties of such quasicrystals are similar to those of disordered metals. The discovery of the Al–Cu–Li icosahedral phase showed that quasicrystals can be at least locally stable and grow under practically equilibrium conditions [13]. At the same time, analysis of diffraction patterns of this and some other quasicrystalline phases revealed the presence in them of specific structural defects — phasons (see Section 2.3 for details). It was supposed that the presence of phasons is an indispensable characteristic of quasicrystalline structures.

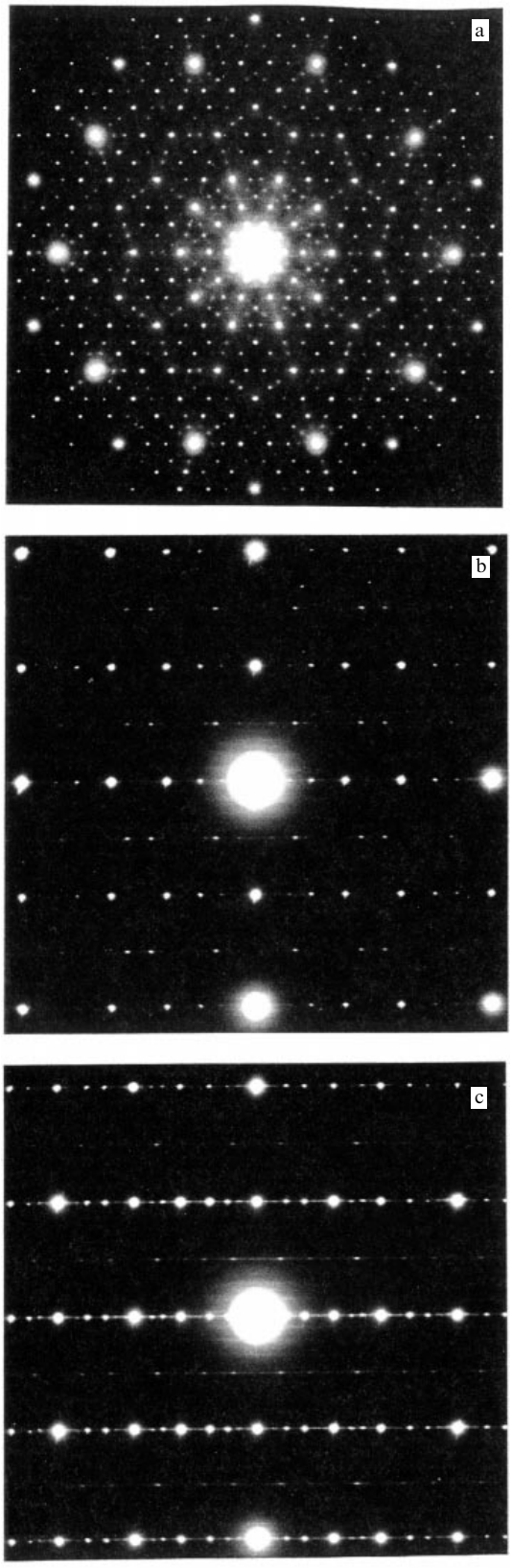

Figure 2. Electron diffraction patterns of the decagonal Al – Ni – Co phase with a high cobalt content: (a) along the symmetry axis of the tenth order, and (b, c) along the symmetry axes A2P and A2D of the second order, respectively (borrowed from Ref. [30]).

New possibilities for experimental investigation into the properties of solids with a quasicrystalline structure opened up after the discovery of phason-free thermodynamically stable phases crystallizing into a face-centered icosahedral (FCI) structure in ternary Al – Cu – Fe, Al – Cu – Ru, and Al – Cu – Os systems [11, 32, 33]. The very first experiments with these phases showed that quasicrystals should be assigned to a separate, very unusual class of solids having properties of both glasses and periodically ordered crystals [34]. An interesting study subject was the thermodynamically stable FCI phase of the ternary Al – Mn – Pd system [35–37], whose Bragg peaks were not broadened by structural defects even in the absence of annealing. Phase equilibriums in this system made it possible to grow single crystals of the icosahedral phase by standard methods and thereby enabled in-depth studies of its structure and properties. The structural perfection of single crystals of Al – Mn – Pd icosahedral phase was confirmed by observation of the Borrmann effect, i.e., anomalous X-ray transmission [38–40].

Today, quasicrystals are known to form in more than 100 systems based on aluminium, gallium, copper, cadmium, nickel, titanium, tantalum, and other elements. As mentioned above, thermodynamically stable icosahedral phases are possible to obtain under normal solidification conditions. Moreover, quasicrystals can be synthesized by such methods as vapor condensation, high-pressure solidification, devitrification of amorphous matter, decomposition of oversaturated solid solutions, interlayer diffusion, ion implantation, the mechanoactivation process, etc. [41–46]. Many methods used to prepare crystalline and noncrystalline phases are also suitable for synthesizing quasicrystals.

The formation of quasicrystals from a melt is, in principle, different from that of metallic glasses readily obtained near the eutectic composition at which none of the crystalline phases is stable and an equilibrium alloy must break down into two or more crystalline phases of different compositions. The chemical separation being under diffusion control, this process is metastable and rapid melt cooling promotes the formation of metallic glass. In contrast, quasicrystals do not form near compositions located close to eutectic ones in the phase diagram. A distinctive feature of equilibrium phase diagrams of systems with quasicrystalline phases is the presence of a peritectic (Fig. 3). These peculiarities of phase diagrams are typical of systems with strong interactions

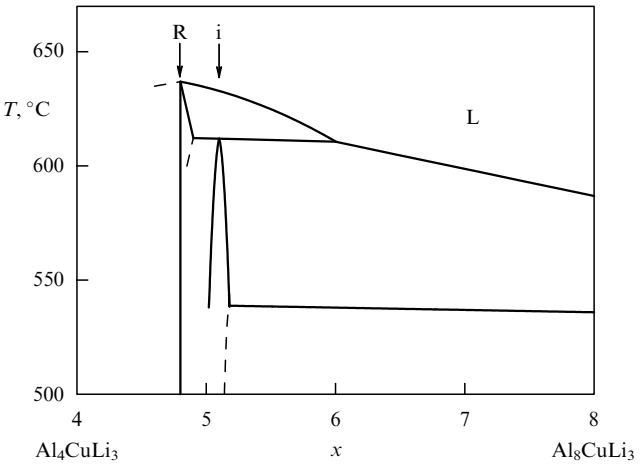

Figure 3. Vertical section through the equilibrium phase diagram of the ternary Al – Cu – Li system along the $Al_4CuLi_3 - Al_8CuLi_3$ line plotted using the results of differential thermal analysis in Ref. [47]: i — icosahedral phase, R — rational approximant with the BCC structure, x — aluminium content, and L — liquid phase domain.

between different atomic constituents and a tendency toward formation of compounds. Quasicrystals are synthesized in these systems through the formation of nucleation centers and their subsequent growth. See Refs [13, 47–50] for more information about the methods of producing various quasicrystals.

One more property being indicative of long-range order in the arrangement of atoms in quasicrystals is the occurrence of faceting of the observed phases. The morphology of a quasicrystalline phase depends on the growth conditions and displays a number of interesting features. Not infrequently, the sole morphological manifestation of a newly synthesized quasicrystalline phase is its point symmetry group [51]. For example, dendrites of the metastable icosahedral phase in the Al–Mn system are shaped like pentagonal dodecahedrons, while dendrites of the thermodynamically stable icosahedral Al–Cu–Li phase have the faceting of the rhombic triacontahedron. Icosahedral quasicrystals in the Al–Pd–Mn system have icosidodecahedral facets. A study of faceting patterns of the icosahedral phase in the Al–Cu–Fe system showed that facets are formed along dense atomic planes in agreement with the requirement of minimum surface stress [52].

While pure metals as a rule undergo crystallization resulting in the formation of simple structures, fusion may yield intermetallic compounds with a rather complex structure. By way of example, two complex crystalline phases of α-$Mn_{12}(Al,Si)_{57}$ and $Mg_{32}(Al,Zn)_{49}$ display local isomorphism with the structure of the corresponding quasicrystals [53, 54]. Each compound constitutes a body-centered cubic (BCC) arrangement of clusters comprising concentric atomic shells with icosahedral symmetry and containing 54 atoms in the former case (icosahedral Mackay cluster) and 44 atoms in the latter (triacontahedral Bergman cluster). Such compounds are called periodic approximants of quasicrystals. There also exists the third type of clusters (Tsai clusters) containing 66 atoms each; the BCC arrangement of such clusters is typical of crystalline alloys like Cd_6Yb, $Zn_{17}Sc_3$ that are periodic approximants of the corresponding binary quasicrystals [55]. Investigations into their structure by high-resolution transmission electron microscopy showed that the cluster structure is typical of quasicrystals, too; however, their clusters are interpenetrating and packed aperiodically. As a result, quasicrystals represent structures with a periodic long-range order and a local cluster structure, rather than simple aggregates of clusters.

The close structural similarity of approximants and quasicrystals is apparent from the similarity of their diffraction patterns [56]. The most pronounced diffraction peaks of crystal approximants are located near analogous peaks of the related quasicrystals. Other evidence of local isomorphism of quasicrystals and appropriate approximants is the coherent orientation coupling between their grains [57]. Quasicrystals frequently form near the approximant composition (Fig. 3); therefore, one of the ways to search for new quasicrystalline compounds is to examine the composition domains near respective compositions of their crystalline approximants [58].

2.2 Methods for structure description

Aperiodic structures giving rise to sharp Bragg reflections, such as a Penrose tiling, were known before 1984 [59]. These structures are essentially characterized by long-range orientation type order. Structures referred to as quasiperiodic coverings or tilings of the plane and space were considered for the purpose of description of quasicrystal diffraction patterns [59, 60].

Let us define the plane tiling by parallelograms [61]. Let n nonparallel vectors $\mathbf{b}_i$ $(i = 1, \ldots, n)$ be given on a plane. Let us then consider all parallelograms formed by vector pairs $\langle \mathbf{b}_i, \mathbf{b}_j \rangle$ $(i \neq j)$. Covering or tiling is such a division of the plane into parallelograms from this set at which they either do not intersect or have a common vertex (or edge). Also, the tiling of space with parallelepipeds can be defined by introducing n vectors $\mathbf{b}_i$ $(i = 1, \ldots, n)$ and considering parallelepipeds formed by vector triads $\langle \mathbf{b}_i, \mathbf{b}_j, \mathbf{b}_k \rangle$ $(i \neq j, k \neq i)$. Tiling of a higher-dimensional space is defined by analogy, while tiling of the straight line is referred to as its division into segments from a given set. A class of quasiperiodic tilings devoid of translation type long-range order is distinguished among the coverings thus obtained. It is such tilings that are used for constructing structural models of quasicrystals.

The most popular among the available models of the structural skeleton of quasicrystalline objects is the two-fragment model based on the quasiperiodic tiling of a straight line, a plane, or space with two elementary structural units. For a one-dimensional quasicrystal, this model leads to the Fibonacci sequence of short (S) and long (L) segments with $S = 1$ and $L = \tau$. In a two-dimensional case, the two-fragment model comprises a Penrose tiling composed of two types of rhombi with acute vertex angles $\pi/5$ and $2\pi/5$ (Fig. 4). In a three-dimensional case, the same model is the generalization of a Penrose tiling formed by rhombohedrons of two types (an Ammann–Mackay network). The absence of translation type long-range order on retention of the long-range orientation type order is a common feature of these two realizations of the two-fragment model. It accounts for the property known in the case of a Penrose tiling as the Conway theorem, according to which any finite configuration of the tiling is met in it quasiperiodically an infinite number of times [62].

There are three principal ways of constructing a two-fragment model, viz. the projection method, the multigrid

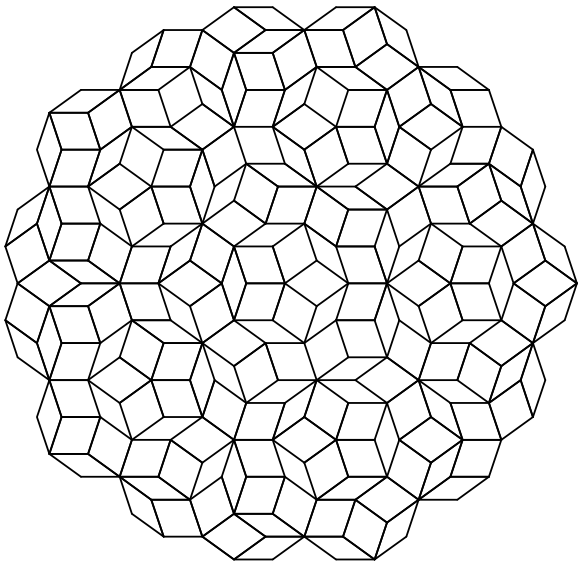

Figure 4. Two-fragment model of a two-dimensional quasicrystal — a Penrose tiling composed of narrow and broad rhombi.

method, and the method using the property of self-similarity of a quasiperiodic structure. The first method is the most convenient for theoretical purposes [3, 63–66]; it was applied to study incommensurably modulated crystals [67, 68]. It is advantageous in that it restores periodicity and allows routine classical analysis of the diffraction pattern using the Paterson function and the structure factor. The quasicrystalline density function can be expanded into the Fourier series in a high-dimensional periodic structure. In such an expansion, the number of basis vectors of an abstract space exceeds the dimensionality of the physical space in which the real quasicrystal exists.

Let us consider application of the projection method to the case of a one-dimensional quasicrystal. To this effect, we shall construct a square lattice with the constant a on a plane with coordinates X_1 and X_2 (Fig. 5) and introduce the second coordinate system $X_\parallel$, $X_\perp$, the axes of which are turned through the angle $\theta = \arctan \tau^{-1}$ with respect to axes X_1 and X_2. We call axis $X_\parallel$ a physical or parallel space, and axis $X_\perp$ an additional or perpendicular space. Let us project onto physical space $X_\parallel$ all sites of the square lattice, which reside within the 'projection tube' (a strip of width $a(\cos\theta + \sin\theta)$ parallel to $X_\parallel$), i.e., projections of a unit cell of the square lattice onto additional space $X_\perp$. In Fig. 5, the projection tube is enclosed between dashed lines parallel to $X_\parallel$. Projections of square lattice sites falling within the projection tube onto physical space $X_\parallel$ determine the positions of lattice sites in a one-dimensional quasicrystal. Distances between the sites of such a lattice are $L = a\cos\theta$ or $S = a\sin\theta$, and their sequence follows the Fibonacci sequence.

Quasicrystalline structures can also be constructed by the section method, with certain advantages for the analysis of experimental diffractograms. Sites of the square lattice in a one-dimensional quasicrystal are decorated by linear segments parallel to additional space $X_\perp$ and equaling the projection of a unit cell of the square lattice onto $X_\perp$ (Fig. 6). Intersections of these segments, called atomic surfaces, with axis $X_\parallel$ determine the positions of lattice sites in a one-

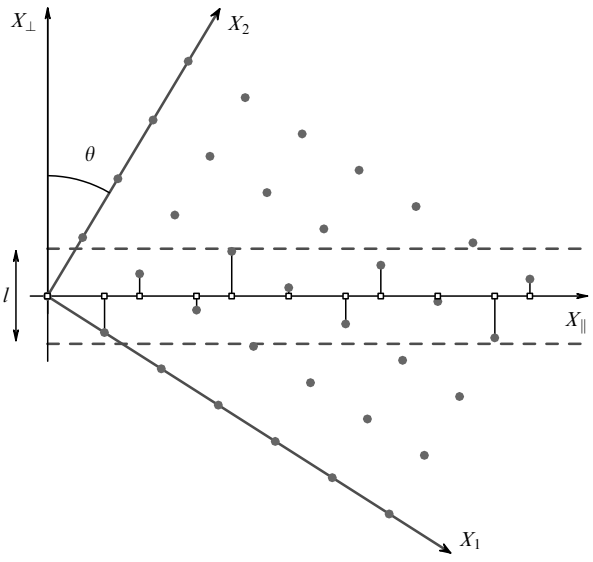

Figure 5. Construction of a one-dimensional quasicrystal (Fibonacci chain) by the projection method; tilt angle of axis $X_\parallel$, i.e., of parallel subspace, with respect to axis X_1 of the two-dimensional square lattice is $\theta = \arctan \tau^{-1}$; projection tube width l equals $a(\cos\theta + \sin\theta)$.

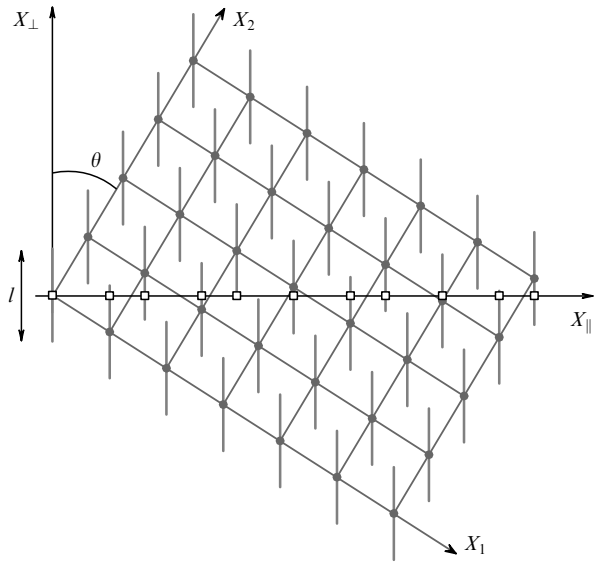

Figure 6. Construction of a one-dimensional quasicrystal by the section method; the length l of atomic surfaces equals $a(\cos\theta + \sin\theta)$.

dimensional quasicrystal. In the general case, a unit cell of the two-dimensional lattice may contain several atomic surfaces; it thereby portrays atoms of other kinds and corresponds to lattices with a basis in the case of periodically ordered crystals.

The Fourier transform of the resulting one-dimensional model of a quasicrystal gives the following expression for the structure factor:

$$S(q_{||}) = \frac{\sin(lq_\perp/2)}{lq_\perp/2}\,, \tag{1}$$

where $q_\parallel$ and $q_\perp$ are the parallel and perpendicular components, respectively, of the reciprocal lattice vector of a two-dimensional crystal, and l is the projection tube width [69]. The projection technique is equally applicable for obtaining the reciprocal lattice of a quasicrystal, with the sole difference being that the size of the projection tube is not fixed. It follows from the expression for the structure factor $S(q_\parallel)$ that the intensity of diffraction spots decreases with a rise of $|q_\perp|$, i.e., as the reciprocal lattice site of the two-dimensional crystal departs from the parallel subspace $q_\parallel$. In the absence of a two-dimensional lattice basis, the square of the structure factor absolute value proportional to scattering intensity depends on $q_\perp$ alone. In the more complicated case of a lattice with a basis, the dependence on $q_\parallel$ also emerges. Taking into account the irrationality of the tangent of the tilt angle of parallel subspace $q_\parallel$ with respect to the axes of the reciprocal lattice of the two-dimensional crystal, the expression for the structure factor of the one-dimensional quasicrystal model shows that the diffraction pattern of the given structure is dense throughout, in the sense that the most intense Bragg reflections corresponding to small $|q_\parallel|$ values are surrounded by reflections of lower intensity, and so forth.

Projection formalism is just as well generalized to the case of two- and three-dimensional two-fragment models of quasicrystals [70, 71]. The integer hyperlattice in a six-dimensional space, as well as three-dimensional physical and additional spaces oriented irrationally with respect to the hyperlattice, is used for constructing the Ammann–Mackay

network. The sites 'close' to the parallel subspace are projected onto it, and this projection constitutes a two-fragment skeleton of the three-dimensional quasicrystal structure. The vertex or the site r_0 of the six-dimensional hyperlattice is present on the projection in the parallel subspace if $n(r_\perp) = 1$, where $n(r_\perp)$ is a function of the shape of the projection of a hyperlattice unit cell onto the perpendicular subspace, equaling unity within the projection and vanishing outside. The inner part of the cell satisfies the condition

$$r = \sum_{i=1}^{6} x_i a_i\,, \quad 0 < x < 1\,, \tag{2}$$

where a_i are the unit vectors of the six-dimensional hyperlattice. Therefore, $n(r_\perp) = 1$ if

$$r_\perp = \sum_{i=1}^{6} x_i a_{i\perp}\,, \quad 0 < x < 1\,; \tag{3}$$

otherwise, $n(r_\perp) = 0$. Vectors $a_{i\perp}$ are directed along the symmetry axes of the 5th order in the icosahedron. Accordingly, the projection tube whose orthogonal section along the additional space is described by nonzero $n(r_\perp)$ values is confined in this space to the interior of the rhombic triacontahedron, i.e., its shape is close to spherical one.

Analysis of diffraction patterns of the Ammann–Mackay network with atoms at lattice sites revealed a number of interesting features [69, 70, 72, 73]. By way of example, diffraction results in a picture of everywhere dense spots, even if only some of them are strong enough, while the remaining ones are essentially suppressed by the dependence of the structure factor on $q_\perp$ in the absence of the basis and on neglecting atomic scattering factors. Indexing of the diffraction patterns is possible by six integer indices using the basis of vectors directed along six symmetry axes of the 5th order in the icosahedron. Reflections in the diffraction pattern may be grouped into two classes: one comprising reflections with the even sum of indices and connected with the powers of τ for the ratio of distances from the pattern center, and the other including reflections with the odd sum of indices and related to the powers of τ^3, in excellent agreement with experiment. These features of diffraction patterns of the Ammann–Mackay network allow it to be used as a basis for structural analysis of real quasicrystals.

The projection method makes it possible to elucidate the presence of long-range order in the Ammann–Mackay network. Indeed, a quasicrystal with a network-like structure can be interpreted as a structure with probabilistic translations or quasitranslations real only for part of the sites. Let us consider the case of a six-dimensional hyperlattice without a basis. Then, the fraction of sites, the displacements from which by a quasitranslation

$$t_\parallel = \sum_{i=1}^{6} m_i a_{i\parallel}\,, \tag{4}$$

where m are integers, and $a_{i\parallel}$ are the projections of the unit vectors of the six-dimensional hyperlattice into the parallel subspace, lead back to the respective site, is given by

$$\frac{\int_\infty n(r_\perp)\, n(r_\perp + t_\perp)\, \mathrm{d}^3 r_\perp}{\int_\infty n(r_\perp)\, \mathrm{d}^3 r_\perp}\,. \tag{5}$$

Here, the following notation was introduced:

$$t_\perp = \sum_{i=1}^{6} m_i\, a_{i\perp}\,, \tag{6}$$

where $a_{i\perp}$ are the perpendicular projections of the unit vectors of the six-dimensional hyperlattice. Notice that expression (5) is the ratio of the volume at the intersection between two triacontahedrons shifted by $t_\perp$ relative to each other to the volume of the triacontahedron itself. The quasitranslation length $|t_\parallel|$ can be made infinitely large practically without a change in $t_\perp$; this suggests undamping of the long-range order.

The multigrid method is analogous to the projection technique but allows working directly in the three-dimensional space; due to this, it is more suitable to elucidate crystallographic aspects [74]. In the context of this method, a Penrose tiling in the form of wide and narrow rhombi makes up a dual pentagrid lattice. Pentagrid G is said to be a totality of five sets of equidistant parallel lines, each set G_j being referred to as a grid:

$$G = \bigcup_{j=1}^{5} G_j\,, \tag{7}$$

$$G_j = x \in R^2\,, \quad x e_j = k_j + \gamma_j\,, \quad k_j \in Z\,, \tag{8}$$

$$e_j = \big(\cos(j-1)\,v\,, \sin(j-1)\,v\big)\,, \quad v = \frac{2\pi}{5}\,, \tag{9}$$

where R^2 and Z are the sets of all real and integer numbers, respectively. Five real parameters γ_j, called grid parameters, determine the position of pentagrid origin and must be chosen to satisfy the relation

$$\sum_j \gamma_j = 0 (\mathrm{mod}\, 1)\,. \tag{10}$$

In this case, no set of three straight lines may intersect at one point. Five unit vectors e_j directed toward the vertices of the regular pentagon define each grid G_j and are called grid vectors. The pentagrid partitions the entire space into a set of polygons. Penrose tiling is obtained by transforming these polygons into vertices of rhombi, meaning that the two lattices, Penrose tiling and pentagrid, are mutually dual. The method of transformation is as follows. A set comprising five integer indices $K_j(x) = [x e_j - \gamma_j]$, $j = 1, \ldots, 5$, where x is taken inside the polygon, and $[x]$ is the largest integer less than or equal to x, is chosen for each polygon. The five indices $K_j(x)$ define the vector

$$P(x) = \sum_{j=1}^{5} K_j(x)\, t_j \tag{11}$$

giving the coordinates of the rhombus vertex (t_j are usually taken to equal e_j). Vertex connectivity is defined in the following way: each intersection point in a multigrid space is common for four polygons that are transformed into four rhombus vertices. The rhombus is obtained by connecting each pair of vertices corresponding to polygons with a common edge. The generation of rhombi for all pentagrid intersection points gives a Penrose tiling formed by wide and narrow rhombi without voids and overlaps. This technique is fully applicable to the generation of the Ammann–Mackay network in a three-dimensional space.

Although both the projection and multigrid methods are suitable for constructing a two-fragment quasiperiodic model of the perfect quasicrystal, it is sometimes (especially for the purpose of numerical computations) more convenient to make use of the structural self-similarity of the model mentioned, the reflection of which is the Conway theorem. This method permits building up a Fibonacci chain of short (S) and long (L) segments by applying the inflation transformation $L \to LS$, $S \to L$. This transformation implies local substitution of all the letters in the chain. The Fibonacci sequence is obtained by applying this transformation, starting from a simple segment, e.g., L. Indeed, one obtains

$$L,\ LS,\ LSL,\ LSLLS,\ LSLLSLSL,\ \ldots\,. \tag{12}$$

In the three-dimensional case of the Ammann–Mackay network, inflation transformation (τ^3 scaling) is performed by matrix $M(\tau^3) = \tau_{\|}^3 P_{\|} - \tau_{\perp}^{-3} P_{\perp} = 2M(\tau) + I$, where

$$M(\tau) = \frac{1}{2}\begin{pmatrix} 1 & 1 & 1 & 1 & 1 & 1 \\ 1 & 1 & 1 & -1 & -1 & 1 \\ 1 & 1 & 1 & 1 & -1 & -1 \\ 1 & -1 & 1 & 1 & 1 & -1 \\ 1 & -1 & -1 & 1 & 1 & 1 \\ 1 & 1 & -1 & -1 & 1 & 1 \end{pmatrix}, \tag{13}$$

I is the unit matrix, $P_{\| ij} = e_{i\|} e_{j\|}$, $P_{\perp ij} = e_{i\perp} e_{j\perp}$, and $e_{i\|}$ and $e_{i\perp}$ are the projections of unit vectors of the six-dimensional hyperlattice into parallel and perpendicular subspaces. Penrose tiling has similar properties.

The section method permits finding the linkage between quasicrystals and their periodic approximants. Let us change the inclination of axis $X_{\|}$ with respect to axis X of a two-dimensional lattice by the ratio of two successive Fibonacci numbers, e.g., $\tan\theta = (3/2)^{-1}$. Then, the points of intersection between axis $X_{\|}$ and atomic surfaces form a periodic structure consisting of identical segments of a one-dimensional quasicrystal (in the present case, $LSLSL$). The structure thus obtained is generally referred to as the 3/2 optimal rational approximant of the quasiperiodic structural Fibonacci chain. The closer the ratio of two successive Fibonacci numbers to τ, i.e., the higher the approximant order, the greater the period of the resulting structure locally isomorphic to a one-dimensional quasicrystal, and the more difficult it is to distinguish such a structure from the one-dimensional quasicrystal, based on diffraction patterns. Obtaining two- and three-dimensional periodic approximants is also associated with rational distortion of orientation of the parallel subspace in a multidimentional space. Thus, a quasicrystal can be regarded as the structural limit of a series of optimal rational approximants with an increasing period. Such representation is extensively used in the analysis of electronic and excitation spectra of quasicrystal lattices.

Very soon after the discovery of icosahedral quasicrystals, a structural model of their skeleton was proposed as an alternative to the two-fragment model; it was later called the icosahedral glass model [2, 75, 76]. As applied to the icosahedral phase, this model can be described as follows. A starting, 'prime' icosahedron is randomly complemented by other icosahedrons provided that no new icosahedron overlaps the existing ones. The icosahedrons are connected via vertices and retain their orientation. With the model implying a random package of icosahedrons, diffraction peaks of such structures have a finite width. The structure factor of the icosahedral glass model is in excellent agreement with experimental data [75]. However, despite the fact that this model does describe certain quasiperiodic phases [77], the discovery of structurally perfect phason-free quasicrystals with narrow diffraction peaks in X-ray patterns [11] cast doubt on the commonality of the structural approach in this model.

2.3 Phasons

To sum up, there are two main approaches to the simulation of the skeleton of an icosahedral quasicrystalline structure, viz. the two-fragment model (quasiperiodic tiling of two elementary structural units) and the icosahedral glass model (random tiling of polyhedrons with prescribed symmetry). The main difference between the two approaches is that the former postulates the existence of quasiperiodic type long-range order, and the latter only short-range order in the arrangement of atoms. Interestingly, these quite different approaches are equally suitable for explaining experimental diffraction data. They are closely related and represent limiting cases of the theory taking into account specific defects in quasicrystals, known as phasons. Phasons represent excitations of the quasicrystal lattice (diffusion modes) caused by local rearrangement of atomic sites. The simplest way to arrive at an understanding of phasons is to proceed from the projection technique. Quasicrystal density can be written down in the form

$$\rho(r_{\|}) = \int_{\infty} \rho(r)\, n(r_{\perp})\, \mathrm{d}^3 r_{\perp}\,, \tag{14}$$

where $\rho(r)$ is the density of a six-dimensional hypercrystal, and $n(r_{\perp})$ is a function of the shape of the elementary hypercell projection onto the perpendicular space. Periodic density $\rho(r_{\|})$ can be expanded in the Fourier series:

$$\rho(r_{\|}) = \sum_{Q} \rho_Q \exp\left(\mathrm{i}Qr\right), \tag{15}$$

where Q are the vectors of the reciprocal lattice of a six-dimensional hypercrystal. Expansion (15) admits additional phases $F_Q(r)$ distorting $\rho(r)$, which are, in turn, expanded into components of parallel and perpendicular spaces, viz.

$$F_Q(r) = Q_{\|} u(r) + Q_{\perp} w(r)\,. \tag{16}$$

Vector fields $u(r)$ and $w(r)$ describe phonons and phasons, respectively. The latter are responsible for the appearance in physical space of local configurations forbidden in the perfect two-fragment model (there are unambiguous local tiling rules for a Penrose tiling and the Ammann–Mackay network [71]). The introduction of phasons becomes possible due to the appearance of additional degrees of freedom in projection formalism. Linear phason fields cause the displacement of diffraction peaks from 'ideal' positions, and nonlinear ones cause their broadening and reshaping [48].

The absence of phasons opens the way to a model of a quasicrystal whose skeleton is described by the Ammann–Mackay network or its low-dimensional analogs. Such a structure arises from the use of a projection tube with a fixed inclination in the high-dimensional lattice. For small restricted random fluctuations of the projection tube inclination around a 'right' value, the structure resulting from the projection is described by the random tiling model. The diffraction pattern of such a structure consists of Bragg peaks found in ideal positions and diffuse scattering from defects [48]. In the case of large and unlimited deviations of

the tube inclination from the right value, the structure resulting from the projection is fairly well described in the framework of the icosahedral glass model. The disorder observed in this case in parallel subspace is called phason strains. Diffraction patterns of structures with phason strains exhibit relatively sharp peaks displaced from ideal positions. Their width increases with increasing perpendicular constituent of the hypercrystal reciprocal lattice vector [48, 78].

Phonon shift relaxation time in quasicrystals, as in ordinary periodically ordered crystals, depends on the speed of sound, and the relaxation time of phason strains (phason diffusion modes) is large (it was experimentally shown to amount to several weeks at room temperature). Phason fluctuations with a characteristic time on the order of 10^2 s are equally possible.

The substantial broadening of Bragg peaks and their displacement from ideal positions observed in experiment are caused by reduced symmetry in quasicrystals due to phason 'frozen-in' modes. In a transition with symmetry reduction in certain directions, the quasicrystal phase becomes commensurate. Incommensurability determined by icosahedral geometry is described by irrational number τ. In a phase with reduced symmetry, the number τ is replaced by some kind of its rational approximation (the ratio of two successive Fibonacci numbers). Analysis of symmetry reduction due to phasons is possible in the framework of the group theory. Maximum subgroups of the icosahedron point group $Y_h = Y \times C_i$ are $T_h = T \times C_i$, $D_{5d} = D_5 \times C_i$, and $D_{3d} = D_3 \times C_i$. Analysis of the spontaneous reduction of symmetry $Y_h = G \times C_i$ involving phason strain fields is usually confined to considering transitions $Y \to G$, where $G = T$, D_5, D_3 (tetrahedral, pentagonal, and trigonal symmetries, respectively). The resulting structure is called a periodic quasicrystal. It is possible to describe in a similar way the Frank–Kasper phases resembling quasicrystals in terms of chemical composition and local atomic order using, instead of τ, its rational 5/3 approximant [79].

Frozen-in phasons were for a long time regarded as irremovable defects inherent in a quasicrystal and forming at the stage of its growth. A similar picture is observed in the case of incommensurably modulated crystals. Their structure is also described with reference to multidimensional space with periodically arranged continuous atomic surfaces. Incommensurate phases also contain phason degrees of freedom which, however, can be described by a linear combination of long-wave phonons. The situation in quasicrystals is different: namely, atomic surfaces are disrupted, which makes phonon and phason displacements independent and does not allow the latter to be presented as atomic displacements in a three-dimensional physical space by analogy with phonon displacements. This fact appears to account for the large relaxation time of phason strains and, hence, for the possibility of their freezing-in. Such systems as Al–Cu–Fe, Al–Cu–Ru, and Al–Mn–Pd exemplify quasicrystals in which phason strains are lacking, as evidenced by the absence of shifts in the diffraction peaks and their almost one order of magnitude smaller width. The main proof of the existence of phason strains is the lack of a systematic dependence of peak width on the parallel constituent $G_\parallel$ of the reciprocal lattice vector in such quasicrystals as Al–Mn and Al–Cu–Li; however, the width shows linear dependence on perpendicular constituent $G_\perp$, which confirms the presence of phason strains in the structure. Phason strains are described by the 3×3 third-rank tensor whose elements are partial derivatives of the phason coordinate with respect to coordinates of physical subspace. In contrast, Al–Cu–Fe, Al–Cu–Ru, and Al–Mn–Pd quasicrystals exhibit a linear dependence of broadening on $G_\parallel$, as in periodically ordered crystals, while its $G_\perp$ dependence is not systematic. Such quasicrystals are called phason-free [33].

Defects of other types, dislocations and surfaces, are more complicated entities than their analogs in periodically ordered crystals due to the incommensurate nature of quasicrystalline phases. Dislocations in quasicrystals have the Burgers vector containing a phason component hampering their mobility because dislocation motion always leaves a phason trace. The necessity of occurrence of screw dislocations for spiral growth of quasicrystals is not obvious. There is a report of an elevated concentration of point defects in quasicrystal objects; for example, it is three orders of magnitude higher in the icosahedral Al–Cu–Fe phase than in typical periodic crystals [80].

2.4 Decoration of structural skeleton

The problem of detecting the decoration of quasicrystal structural skeleton by atoms or their clusters is analogous to identification of the basis and the atomic positions in a unit cell of a periodically ordered crystal, provided the spatial group and periods of the lattice are known. As mentioned above, the two-fragment model is the most popular one for the quasicrystal structural skeleton. Therefore, certain researchers have tried to determine the concrete positions of atoms in this skeleton by structural analysis using the Paterson function. The three-dimensional Paterson function $P(r_\parallel)$ is defined as a Fourier transform of diffraction intensities obtained in experiment, viz.

$$P(r_\parallel) = \sum_i I(S_i) \exp(-2\pi S_i r_\parallel), \tag{17}$$

where summation is performed over all reflections with scattering vectors S_i. It should be noted that $P(r_\parallel)$ provides the maximum amount of information obtained without any additional assumptions. Moreover, the Paterson function may be regarded as a three-dimensional pair correlation function providing both information on permitted interatomic distances in the structure and angular information. Computation of $P(r_\parallel)$ in the parallel space yields an aperiodic function; comparison of its maxima with the theoretical quasicrystal skeleton gives one decoration model or another. However, practical application of this procedure encounters difficulties in deciphering the Paterson function caused by structure quasiperiodicity. From this standpoint, calculation of the six-dimensional Paterson function appears more preferable [81] because it permits finding the basis of the six-dimensional hyperlattice and the shape of atomic surfaces in the six-dimensional space, i.e., three-dimensional 'orthogonal' objects analogous to the segments depicted in Fig. 6. Notice that if the shape of atomic surfaces in the perpendicular space differs from rhombic triacontahedron, the skeleton of the projected structure is no longer described by the Ammann–Mackay network and implies more complicated objects [82].

Atomic positions in a quasicrystal can be found by comparing them with related crystalline phases, such as periodic approximants, making use of their local structural isomorphism. In the case of the crystalline Al–Cu–Li R-phase, a unit cell can be divided into acute rhombohedrons and rhombic dodecahedrons (composed of two 'prolate' and

two 'oblate' rhombohedrons) with the specified decoration of these polyhedrons. Taking into account the rational inclination of the projection tube in the six-dimensional hyperlattice for obtaining periodic approximants, this decoration may prove suitable for a description of the structure of a stable icosahedral Al – Cu – Li quasicrystal, too. Topological problems make difficult verification of this hypothesis. Theoretical analysis of a somewhat simplified variant of this decoration yields diffraction patterns similar to experimental ones [81]. In order to describe the structure of the icosahedral phase in the Al – Cu – Li system, the authors of Ref. [83] proposed decorating rhombohedrons of the Ammann–Mackay network (enlarged by the factor τ^3 compared with the experimentally found minimal size) by large Pauling triacontahedrons with a complex atomic structure that are encountered in the description of the R-phase. Calculated diffraction patterns were consistent with experimental ones, but the presence of weak 'theoretical' peaks absent in experiment implies the necessity of more exact definition of this model.

Combination of two above approaches to the interpretation of quasicrystal atomic structure, i.e., its analysis using the Paterson function and comparison with the decoration of periodic approximants, constitutes the most general structural approach. Indeed, computation of the Paterson function for the crystal approximant allows the atomic basis of a six-dimensional hyperlattice to be determined. In such a case, the quasicrystal structure in the parallel space is a function of tube reorientation and a projection of the structure with the basis onto the physical space. This approach was used in Refs [84, 85] where the α-phase of the Al – Mn – Si system was regarded as the rational 1/1 approximant of the icosahedral quasicrystal. The authors obtained the atomic structure of the icosahedral phase in the Al – Mn – Si system by deducing the atomic decoration of the hyperlattice from the Paterson function and changing the inclination of the projection tube by an irrational one. Despite good agreement with experiment in terms of diffraction patterns, this model contained many nonphysically short interatomic distances. Substitution of the polyhedral atomic surfaces for initially used spherical ones brought about reasonable interatomic distances, adequate atomic density, and local structure similar to that of α – Al – Mn – Si containing a large number of Mackay icosahedral clusters. Such a procedure was applied to other quasicrystalline phases, too [86, 87].

One more method designed to interpret atomic structure directly from a concrete variant of the basis of a six-dimensional hyperlattice has been extensively used in addition to the above approaches. In application to the structural skeleton of the Ammann–Mackay network, it consists in exhausting different bases of a six-dimensional hyperlattice and calculating diffraction patterns until they agree well with experimental ones. In a three-dimensional parallel space, this procedure leads to the decoration of rhombohedrons by atoms of different kinds. However, this approach is laborious due to the specific structural features of quasicrystals and should be used only when a given skeleton is shown (by any of the above methods) to be readily decorated by atoms and fairly well describes the quasicrystal structure of the system of interest. By way of example, it was shown that the description of the skeleton of an icosahedral quasicrystal in the Al – Mn system by the Ammann–Mackay network is sufficient to adequately characterize the atomic structure with simple decoration [88].

Determination of the atomic arrangement in quasicrystalline phases remains a challenging problem because the accuracy of basis interpretation for quasicrystals is still much lower than for periodically ordered crystals [89]. It has been shown that both approximants and quasicrystals exhibit a cluster structure. For three-dimensional structures, the three types of clusters described above make up an icosahedral quasicrystal and decorate the spatial aperiodic lattice according to certain overlap rules. Column clusters form two-dimensional quasicrystal structures. The positions of the atoms inside clusters are fixed, although chemical disorder is possible. Gummelt [90] proposed constructing two-dimensional quasicrystal structures by the quasicell method with the laying of planes into a single decagonal 'two-color' structural block. This procedure is equivalent to the construction of a Penrose tiling in conformity with the well-defined rules of cluster overlapping.

3. Electronic spectrum and structural stability

The probability of formation of the icosahedral phase during rapid cooling from the homogeneous (liquid) state was considered in the framework of the Landau theory of phase transitions before the discovery of quasicrystals. Alexander and McTague [91] expanded the free energy of a weakly inhomogeneous system in powers of density, restricting consideration to the third- and fourth-order terms, and arrived at the conclusion that the icosahedral structure is thermodynamically inferior to body-centered cubic (BCC) or hexagonal structures. They found the BCC structure to be more advantageous. Later on, Mermin and Troian [92] included the fifth-order terms in the analysis, as well as Kalugin, Kitaev, and Levitov [63] considered instability of the homogeneous state relative to the formation of a density wave with icosahedral symmetry, taking into account two wave vector stars corresponding to the vertices and edges of the icosahedron. Their results suggested a higher probability of formation of the icosahedral phase.

Taking account of the entropic contribution may substantially diminish free energy. The entropy of a random quasicrystal is greater than that of regular quasicrystals having a different inclination of the three-dimensional space with respect to the six-dimensional lattice. On the other hand, assuming the regular quasicrystal to be in the ground state, the introduction of phasons in the structure must be accompanied by a rise in the total energy due to the appearance of configurations absent in the ground state. Competition between these contributions has a marked effect on the real structure of quasicrystals.

Microscopically, the binding energy depends on two main contributions: direct ion–ion interaction, and indirect ion–ion interaction mediated through valence electrons. Analysis of the electrostatic contribution to the binding energy of an 'ideal' icosahedral quasicrystal structure shows that the Madelung constant for decorated Ammann–Mackay networks is significantly smaller than for densely packed structures [93–96]. Accordingly, the contribution from direct electrostatic interaction between ions to the binding energy is small compared with that of indirect ion–ion interaction, with structural stability being essentially dependent on the peculiarities of electronic spectra.

The difficulties encountered in the analysis of electronic spectra and electron transport in quasicrystals are primarily due to the inapplicability of the Bloch theorem. For a one-

dimensional quasicrystal or Fibonacci chain in the strong-coupling approximation, site energies or hopping integrals are parameters that quasiperiodically 'intermix' according to the rule dictated by the Fibonacci sequence. In the strong-coupling approximation, the problem is solved analytically. In this case, the spectrum has a self-similar structure of energy gaps called the 'devil's staircase', and the total band width tends toward zero in accordance with the power law $B \sim N^a$ as the size of the system increases. The energy spectrum constitutes a Cantor set of Lebesgue measure zero. To recall, a set lying on the number axis is referred to as the set of Lebesgue measure zero if for any $\varepsilon > 0$ this set is covered with a finite or countable system of intervals, the total length of which is smaller than ε. Another feature of the one-dimensional quasicrystal electronic structure is the critical behavior of electron wave functions that are neither delocalized nor localized. In a classification according to the normalization integral, the wave function $\psi(r)$ is localized if the integral $\int_\infty |\psi(r)|^2 \, dr$ converges, and delocalized or extended if $\int_{|r|<R} |\psi(r)|^2 \, dr \sim R^d$, where d is space dimension, and, finally, critical if the normalization integral is not described by two above-mentioned cases. In conformity with this definition, the power-law wave function $\psi(r) \sim |r|^{-\alpha}$ is localized if $\alpha > d/2$. Therefore, electrical resistance of a one-dimensional quasicrystal shows a power-like dependence on length [63, 97, 98].

Properties intrinsic in one-dimensional quasicrystals are not necessarily common to higher-dimension quasiperiodic objects. The peculiarities of one-dimension periodic systems are well-known in the Anderson localization problem: wave functions always remain localized at an arbitrarily small degree of disorder. At the same time, wave functions for the Fibonacci sequence are always critical. Even more important is the fact that the Fibonacci chain is considered in a problem implying a distribution of two-valued potentials or hopping integrals over a topologically regular lattice. Real quasicrystals are topologically nonperiodic in a three-dimensional space, and certain results obtained for the Fibonacci chain are characteristic of one-dimensional systems alone.

Investigations of a two-dimensional Penrose tiling in the framework of strong-coupling approximation demonstrated that the electronic spectrum has no universally dense self-similar gap structure characteristic of the Cantor set but possesses a singular part, i.e., it is nonsmooth. Smooth spectra are those in which interlevel intervals ΔE in the thermodynamic limit depend on the system size as $\Delta E \sim 1/N$; in nonsmooth ones this dependence assumes the form $\Delta E \sim 1/N^\beta$, where $\beta \neq 1$ [99–101]. Most wave functions for the two-dimensional quasicrystal model are critical. The length dependence of conductance was studied for so-called semiperiodic Penrose tilings obtainable as periodic arrays of infinitely long quasiperiodic strips. Conductance underwent a power-like decrease with increasing strip length. The energy dependence of conductance is subject to strong oscillations, probably due to the spectral nonsmoothness of two-dimensional quasicrystals [99–101]. The random introduction of topological configurations (phasons) forbidden for Penrose tilings obliterates the peculiarities of the density of electronic states in two-dimensional perfect quasicrystals and thereby increases conductance at certain energy values when the density of states of the perfect system is close to zero. It may be a cause of conductance growth in real quasicrystals with increasing the density of random phasons [102].

Electronic spectra of three-dimensional (icosahedral) quasicrystals were explored in Refs [103, 104]. The quasicrystal was regarded as the limit of a sequence of rational periodic approximants with the growing period. It was shown for the Ammann–Mackay network with central and vertex decorations of rhombohedrons in the strong-coupling approximation that the wave functions are critical near the Fermi energy. The spectrum does not contain a self-similar gap structure and its Lebesgue measure is nonzero; however, it involves a small singular part. The root energy dependence of the spectrum characteristic of periodic structures undergoes distortion and reaches a peak with increasing the order of the approximant as it tends to the quasicrystal. Wave functions near the Fermi level are critical and their envelope decreases with distance following the power law.

A characteristic feature of the electronic spectrum of icosahedral quasicrystals is the presence of a pseudogap in the density of states at the Fermi level, the feature demonstrated by calculations of electronic spectra, observations of specific heat and photoemission, and nuclear magnetic resonance (NMR) and tunneling experiments. The main cause behind pseudogap formation in the electronic spectrum is the points of contact of the Fermi sphere with the Brillouin zone edges. The pseudogap results from interference between electronic waves and wave vectors $\mathbf{K}$ and $\mathbf{K} + \mathbf{G}$. Here, $\mathbf{G}$ is the reciprocal lattice vector corresponding to Bragg reflection and satisfying the condition $|\mathbf{G}| = 2k_F$, where k_F is the radius of the Fermi sphere. Strictly speaking, Brillouin zones cannot be constructed for aperiodic crystals, but Brillouin pseudozones corresponding to the first strong Bragg reflections can be introduced for quasicrystals. Due to the high multiplicity factor of such reflections, the Brillouin pseudozones are almost spherical in shape; accordingly, the pseudogap is wider and deeper than in crystal approximants [105–107]. Pseudogaps occur in amorphous and crystalline alloys, too, where they are not as apparent as in quasicrystals. The landing of the Fermi level in the pseudogap at a certain number of valence electrons per atom stabilizes the structure. It is the so-called Hume-Rothery rule, well known from the electron theory of alloys, whose applicability to quasicrystals was considered in Refs [108–112, 55].

As known empirically, stable icosahedral quasicrystals form when a mean number of valence electrons per atom (e/a) is close to 1.7 or 2.1. Quasicrystals containing no transition elements, such as Al–Li–Cu, Zn–Mg–R (R = Y, Gd, Tb, Dy, Er, Ho) systems, belong to the quasicrystal family with e/a = 2.1, for which the Fermi sphere with diameter $2k_F$, computed from the electron density, is close to reciprocal lattice vectors (222100) and (311111). However, stable binary quasicrystals $Cd_{5.7}Yb$ and $Cd_{17}Ca_3$ are realized at e/a = 2. Photoemission experiments and theoretical calculations indicate that the Fermi level in these objects does not coincide with the minimum of the observed pseudogap and that the main cause responsible for pseudogap formation is spd-hybridization of electronic states, rather than interaction between the Fermi sphere and Brillouin pseudozone [55]. Each of the three above e/a values corresponds to a fundamental cluster of atoms making up respective quasicrystals and approximants (see Section 2.1). The pseudogap is not a universal property of all quasicrystals. For example, it was not revealed in decagonal quasicrystals, probably due to periodic packing of quasicrystal planes; naturally, its presence does not compromise the significance of the Hume-Rothery criterion.

In addition to the pseudogap, the electronic spectrum of quasicrystals is characterized by a fine peak structure with a gap width on the order of 10–50 meV as shown in Ref. [101] and confirmed by tunneling [113–115] and NMR [116] experiments. Such a structure of the spectrum suggests the existence of almost dispersionless flat energy bands and, accordingly, a low mobility of current carriers in quasicrystals.

4. Lattice excitations

The problems of vibrational eigenmodes and one-electron states lead to identical equations, which permits using the results of studies concerned with the behavior of noninteracting electrons in quasicrystals. No exact solutions have been reported in the literature, barring a one-dimensional case [97, 117]. All that has proved possible to show in two- and three-dimensional cases is the irrelevance of the hypothesis of quasi-Bloch states in quasicrystals [118]. Bloch states in periodically ordered crystals are localized in the momentum space and therefore resemble states occupied by free particles. Eigenstates in quasicrystals are never localized in k-space. They are always subject to internal decay, although the rate of this process in the weak-scattering limit is negligibly low. Despite the similarity of the equation for vibrational eigenmodes and the one-electron Schrödinger equation, they are different in one important aspect. While the scale of momenta intrinsic to occupied electronic states is given by Fermi momentum p_F and cannot be chosen arbitrarily, in the case of lattice excitations there is always a long-wave limit where the quasiperiodicity of the potential does not play any significant role.

As mentioned earlier, the exact solution to the problem of vibrational eigenmodes [119] and one-electron Schrödinger equation [118] was found for the one-dimensional model of the quasicrystal. This solution was obtained using the formalism of transfer-matrices relating displacements of two neighboring atoms in the case of vibrational modes or two independent solutions of the Schrödinger equation, e.g. Ψ and Ψ'. The main result of the relevant theory is that the universality class of the problem is determined by the value of the single parameter J [117, 98]. The standard choice of this parameter is a half-trace of the multiplicative commutator of transfer-matrices corresponding to specified sites in the Fibonacci chain. Parameter J never takes values smaller than one, and the case when it equals unity corresponds to the universality class of the periodic chain. Given below is the expression for the parameter J in the case when the Fibonacci chain consists of atoms with two different masses, m_1 and m_2, and elastic forces between the neighboring atoms are identical. The transfer-matrix relating displacement vector $\mathbf{u}_n = (u_{n-1}, u_n)$, where u_i is the vibration amplitude of the ith atom, with displacement vector $\mathbf{u}_{n+1} = (u_n, u_{n+1})$ can be written for the mode of a given frequency ω in the form

$$T_n = \begin{pmatrix} 0 & 1 \\ -1 & 2 - m_n k^{-1} \omega^2 \end{pmatrix}. \qquad (18)$$

Here, m_n is the atomic mass at site n, and k is the elastic constant. Taking into account ω^4-order terms, the half-trace of the multiplicative commutator of transfer-matrices at two adjacent sites 1 and 2 is written down as

$$J = \frac{1}{2} \operatorname{tr}(T_1 T_2 T_1^{-1} T_2^{-1}) = 1 + \frac{(m_1 - m_2)^2}{2k^2} \omega^4 . \qquad (19)$$

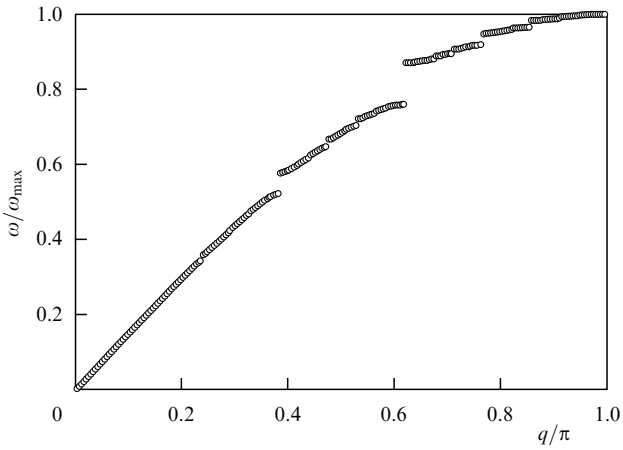

Figure 7. Frequencies of vibrational eigenmodes of a Fibonacci chain consisting of 233 atoms with two different masses; mass ratio is 3/2 (taken from Ref. [120]).

Parameter J tends toward unity as frequency decreases. It reflects the fact that local details of the quasicrystal structure become less significant in the long-wave limit.

Although the lattice excitation spectrum of a one-dimensional quasicrystal has measure zero, as in the case of the one-electron Schrödinger equation for the Fibonacci chain, in the long-wave limit it looks continuous because gap widths become smaller than the separation between eigenmodes of a finite-length chain. Figure 7 depicts eigenmode frequencies of the Fibonacci chain consisting of 233 atoms with the mass ratio 3/2 as a function of pseudowave vector q defined as eigenmode nodal density [120]. Such a definition is a natural generalization of the wave vector in the case of a quasiperiodic chain because node density is proportional to the wave vector in the case of a periodic chain. The $\omega(q)$ plot in Fig. 7 exhibits only the most important gaps. It is known from the exact solution for the Fibonacci chain that the widths of such gaps in the spectrum are proportional to $\sqrt{J-1}$, i.e., the square of frequency [117, 98].

Calculations of the dynamic response of different three-dimensional models of quasicrystal lattices were made for both rational approximants with large unit cells and large quasicrystal clusters. Theoretical analysis of the models of rational approximants with large unit cells containing up to 10^5 atoms revealed not only acoustic modes near the most intense Bragg peaks but also the hierarchical structure of excitation branches of a lattice with pseudogaps that reaches the lowest frequencies and results in deviation from the usual, i.e., quadratic in frequency, density of vibrational modes even at relatively low frequencies [121]. The introduction of structural defects into such a model therewith smears out the peculiarities of the vibrational mode density. Interestingly, dispersion of acoustic branches becomes increasingly more isotropic and transverse velocities of sound tend toward one and the same value with increasing approximant order. In quasicrystals with icosahedral symmetry, the law of dispersion of acoustic oscillation branches is isotropic, and transverse acoustic branches are degenerate.

Experimental studies of quasicrystal lattice dynamics by inelastic neutron and X-ray scattering methods included different systems, such as icosahedral Al–Li–Cu, Al–Cu–Fe, Al–Mn–Pd, Y–Mg–Zn, Zn–Mg–Sc phases [122–130], and the decagonal Al–Ni–Co phase [131].

Comparative analysis of lattice excitation spectra of the icosahedral Zn – Mg – Sc phase and its rational 1/1 approximant Zn – Sc was undertaken in Ref. [130]. Of all icosahedral phases, that of Al – Mn – Pd was most thoroughly investigated in terms of lattice dynamics due to the possibility of growing large single crystals of high structural quality. The main results of these investigations [126, 127] are reviewed below.

In the long-wave limit, experimentally examined excitations of an icosahedral lattice are well-defined acoustic modes with a width matching the resolution power of the spectrometer. The acoustic modes are isotropic and their velocities are in excellent agreement with the results of ultrasonic measurements performed on the same Al – Mn – Pd specimens. It should be noted that unambiguous correspondence between the measured energy spectrum of scattered neutrons and a selected branch of the excitation spectrum (dispersion relation) can be established only in the low-frequency region. In the region of intermediate frequencies, each measured signal is possible to associate with a certain strong Bragg peak. Therefore, the choice of strong Bragg peaks as 'band' centers permits describing experimental results in the language of dispersion relations.

In the frequency region above 2 THz, the width of a transversely polarized acoustic mode begins to rapidly grow, while the slope of the corresponding dispersion relation decreases. In the region above 3 THz, a longitudinal acoustic mode becomes virtually dispersionless. The width of transversely polarized acoustic modes starts to increase for wave vectors $q > 0.35$ Å^{-1} and reaches roughly 1 THz at $q = 0.65$ Å^{-1}, when the corresponding dispersion relations substantially deviate from the linear law (Fig. 8). Such a behavior of lattice excitation spectra characteristic of all icosahedral quasicrystals precludes measurement of dispersion laws at frequencies above 6 – 8 THz. Notice, however, that measurements of the generalized vibrational mode density $g(\omega)$ by the time-of-flight neutron inelastic scattering method are feasible only at frequencies of up to 12 – 14 THz [132]. Four 1-THz wide dispersionless modes were detected in the frequency range from 2 to 6 THz, in addition to acoustic modes.

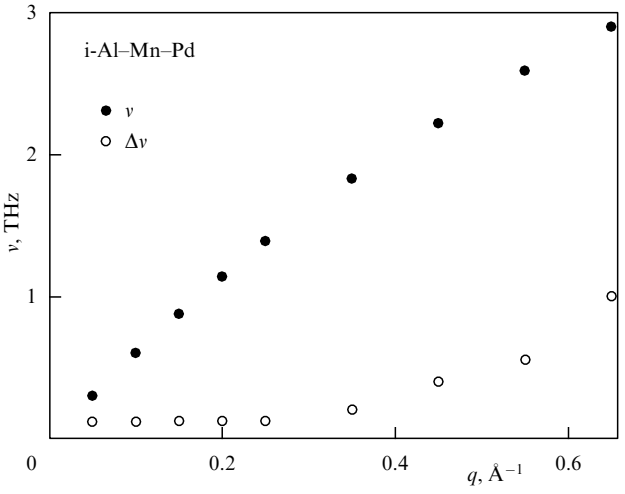

Figure 8. Frequency v and width Δv of the transversely polarized acoustic mode in the icosahedral Al – Mn – Pd phase as a function of wave vector q (taken from Ref. [127]).

The spectra $\omega(\mathbf{q})$ of lattice excitations of the decagonal Al – Ni – Co phase for certain symmetric directions measured by the inelastic neutron scattering method using a three-axis spectrometer at 300 K were reported in Refs [131, 133]. Two transverse and two longitudinal modes propagating parallel to the crystallographic directions $[11\bar{1}\bar{1}0]$ and [00002] were observed near Bragg peaks (00002) and $(11\bar{1}\bar{1}0)$, respectively, with their polarization vectors laying in the plane formed by directions [00002] and $[11\bar{1}\bar{1}0]$ [131]. The speeds of sound in the decagonal Al – Ni – Co phase, derived from $\omega(\mathbf{q})$ in the long-wave limit, are in excellent agreement with components c_{ij} of the elastic modulus tensor found by ultrasonic resonance spectroscopy [134, 135]. As shown in Ref. [131], dispersion of acoustic excitations is isotropic within the experimental error for wave vectors $|\mathbf{q}| < 0.55$ Å^{-1}. This finding is in qualitative agreement with the results of c_{ij} measurement, showing that changes in the speeds of sound $v_i(\theta)$ with a polar angle θ between the acoustic wave vector and the decagonal axis do not exceed 13% [134, 135]. At the same time, the experimental data reported in Ref. [131] are in conflict with theoretical studies of lattice excitations in decagonal quasicrystals, exemplified by the Al – Mn phase [136]. The theory predicts strongly anisotropic dispersion for lattice excitations spreading in the quasiperiodic plane and along the periodic direction.

The local cluster structure affects the lattice dynamics of quasicrystals in a certain way and is different in quasicrystals with Mackay and Bergman clusters. In the former, the generalized density $g(\omega)$ of vibrational modes is smoother and structureless, containing one or two bands of the phonon spectrum. In the latter, the structured short-wave part of the spectrum includes a few energy subbands due to differences in short-range interatomic interaction. Differences between lattice excitation spectra of quasicrystals and their rational approximants are insignificant [130]. In $g(\omega)$ spectra, peak positions and intensities are somewhat different: namely, structures with Bergman clusters for approximants (unlike structures with Mackay clusters) show narrower peaks compared with quasicrystals.

5. Physical properties of quasicrystals

Most quasicrystals are intermetallic alloys with properties essentially different from those of crystalline and amorphous phases with a similar composition. There is a wealth of experimental data on quasicrystal properties summarized in good reviews and monographs (see, e.g., Refs [24 – 26, 28, 107, 137]). These specific properties are determined by aperiodic long-range order and local atomic structure. The influence of these factors becomes apparent upon comparing the properties of quasicrystals and approximants. Section 5 deals with their electron and thermal transport, superconductivity, magnetic and mechanical properties. We shall first consider electron transport.

5.1 Electron transport

The electrical resistivity of quasicrystals is smaller than that of insulators and doped semiconductors, but greater than in metals and the corresponding periodic approximants. The carrier concentration determined by measurements of the Hall effect (the Hall coefficient for quasicrystals may be sign-changing and temperature-dependent) is on the order of $10^{20} - 10^{21}$ cm^{-3}. This raises the question of the state of electrons in quasicrystals. The resistivity $\rho_{4.2\,\mathrm{K}}$ of icosahedral

quasicrystals at the liquid-helium temperature varies from 70 μΩ cm in Al–Mg–Cu to 2 Ω cm in polycrystalline Al–Pd–Re samples. It does not exceed 2000–4000 μΩ cm at 300 K, and 3000–6000 μΩ cm at 2 K in single crystals of the icosahedral Al–Pd–Re phase.

As a rule, the temperature coefficient of resistivity $d\rho/dT$ of icosahedral quasicrystals has a negative value. The icosahedral Al–Mg–Cu phase is an exception in that its resistance is practically independent of temperature. The temperature coefficient of resistivity of decagonal quasicrystals is negative only in quasicrystal planes, and positive ($d\rho/dT > 0$) in the periodic direction; also, resistivity ρ_p in the periodic direction is much lower than along the quasiperiodic plane, ρ_q. Contributions from residual resistivity $\rho(0)$ at zero temperature and the temperature-dependent part $\Delta\rho(T)$ are not additive (the additivity of these contributions for periodically ordered metals is the essence of the well-known Matthiessen's rule). In the case of icosahedral quasicrystals, conductivities instead of resistivities are summed up: $\sigma(T) = \sigma(0) + \Delta\sigma(T)$.

Variations of resistivity in icosahedral quasicrystals with temperature are usually characterized by the ratio $R = \rho_{4\,K}/\rho_{300\,K}$. The value of R for practically all icosahedral quasicrystals ranges from 1.1 to 4. For example, for stable Al–Cu–Li and Al–Cu–Ru phases, one has $R \approx 2$. An exception is the icosahedral Al–Pd–Re phase for which R varies from 2 to 250 depending on composition and conditions of synthesis (Fig. 9) [138]. In single crystals of this phase, one finds $R \approx 2$. Disorder in quasicrystals causes resistivity (especially low-temperature resistivity) to decrease. A perfect quasicrystalline object should have zero conductivity $\sigma(0)$ but it is actually finite due to local chemical disorder. Most icosahedral quasicrystals have $\sigma(T) \sim T^{\beta}$ with $1 \leqslant \beta \leqslant 1.5$ in the temperature range above 20 K. At low temperatures, the temperature-dependent contribution $\Delta\sigma(T)$ to conductivity behaves like $T^{1/2}$, probably by virtue of correction arising from electron–electron interaction. This issue is also extensively discussed in the literature with reference to magnetoresistance experiments [139].

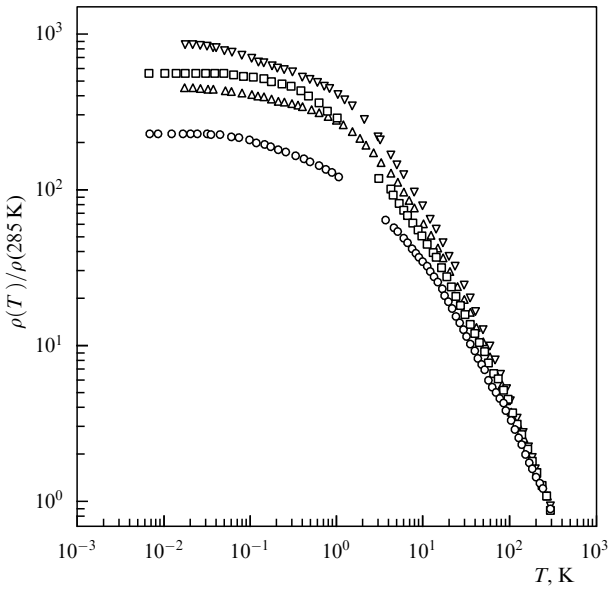

Figure 9. Temperature dependence of resistivity in polycrystalline samples of icosahedral Al–Pd–Re alloys with different $\rho_{4\,K}/\rho_{285\,K}$. (Reprinted with permission of Rodmar M, Zavaliche F, Poon S J, Rapp O *Phys. Rev. B* **60** 10807 (1999). Copyright 1999 by the American Physical Society).

Polycrystal samples of the icosahedral Al–Pd–Re alloy with large R at low temperatures behave as disordered conductors near metal–insulator transition. In Al–Pd–Re alloys with small R, one finds $\Delta\sigma(T) \sim T^{1/2}$. Specimens with $R > 10$ for $T < 10$ K are characterized by the dependence $\Delta\sigma(T) \sim T^{1/3}$ inherent in the $\Delta\sigma(T) > \sigma(0)$ regime in the critical region of metal–insulator transition. Variable-range-hopping conductivity $\sigma(T) = \sigma_0 \exp[-(T_0/T)^p]$ with $p = 1/4$ (Mott law) or $p = 1/2$ (Efros–Shklovskii law) typical of insulators, is observed at larger R [140]. At constant density of states at the Fermi level for transitions with phonons, one has $p = 1/(d+1)$ (Mott law), where d is the system's dimension ($p = 1/2$ when electron–electron interactions are taken into account). Characteristically, neither the icosahedral phase of Al–Pd–Re single crystals nor any other quasicrystalline phase undergoes transition to the state with variable-range-hopping conductivity.

Resistivity is known to correlate with peculiarities of quasicrystal electronic spectra. For alloys with $\rho < 500$ μΩ cm, resistivity correlates with the depth of the pseudogap at the Fermi level. For $\rho > 500$ μΩ cm, the presence of a pseudogap is insufficient, and high resistivity is due to the low mobility of current carriers, i.e., to the localization effects. The higher resistivity of quasicrystals compared with ordinary metals and doped semiconductors is attributable to the peculiarities of chemical bonds and structure, which manifest themselves as specific local cluster structure and aperiodic long-range order. The latter property is responsible for the specific dependence on defectiveness and the negative sign of the resistivity temperature coefficient in quasicrystals. Indeed, approximants with such short-range order as a rule have $d\rho/dT > 0$, and $d\rho/dT$ changes sign only for $\rho > 500-1000$ μΩ cm and considerable chemical disorder, i.e., substitution disorder in the cluster [105]. As is known, $d\rho/dT$ in typical disordered metallic alloys becomes negative for $\rho > 150$ μΩ cm; at such resistivity values a disorder-related localization becomes apparent [141]. The absence of the Drude peak in the optical conductivity of quasicrystals also suggests localization of electronic states due to disorder (see Section 5.2). Moreover, this peak is lacking in approximants with large ρ values and marked chemical disorder, and can be expected to emerge at temperatures above the Debye temperature θ_D [142], but this conjecture needs verification in future experiments.

There is no consistent theory of electron transport in quasicrystals, the main cause being inapplicability of the Bloch theorem to these objects. Most speculation to this problem remains a matter of qualitative reasoning. The following two scenarios are feasible in the analysis of electron transport in quasicrystals: the cluster-based approach, and scattering in the aperiodic potential field. The available cluster models qualitatively explain the nature of high resistance in quasicrystals. One type of such models is exemplified by the chemical localization model suggesting a blockade of part of the 'potentially metallic' electrons by chemical bonds, as in two-component melts with one component being an alkali metal [143, 144]. The other type is self-similarity cluster models [145].

The electronic properties of a real system with aperiodic potential are equally possible to describe in terms of the model of the multicomponent Fermi surface containing a large number of electron and hole pockets. This model is based on

the so-called band structure hypothesis that was applied to the analysis of optical conductivity spectra of icosahedral Al–Cu–Fe quasicrystals [146]. This model was developed for the description of temperature dependence of electrical conduction and thermo-electromotive force in the work of Burkov, Varlamov, and Livanov [147, 148]; thereafter, it was employed to describe high-temperature conductivity and electron localization in quasicrystals [149]. The model permits successfully applying the quasiclassical Bloch–Boltzmann theory of electron transport for the description of the temperature dependence of conductivity and its dependence on defectiveness, for describing localization effects in the $k_F l > 1$ regime, where l is the mean free path of carriers, and for qualitatively taking account of strong localization at $k_F l \sim 1$. The logic behind this model is as follows. When a quasicrystal is considered as the structural limit of a sequence of periodic approximants with increasing period, the Fermi surface becomes increasingly multicomponent and contains more and more electron–hole pockets. At low temperatures, only intravalley scattering with small momentum transfer is possible. The probability of intervalley transitions increases with temperature, which accounts for the temperature-dependent enhancement of conduction. At $k_F^i l \sim 1$, where k_F^i is the Fermi momentum in the ith valley, the Ioffe–Regel criterion is met and localization of electrons with the characteristic temperature-related behavior of conductivity becomes possible. The model predicts a rise in conductivity with increasing the degree of defectiveness and also proves useful for explaining the optical conductivity spectra [146], thermal conductivity [150], and diamagnetism [151] of quasicrystals.

The Hall (R_H) and Seebeck (S) coefficients of icosahedral phases have large absolute values and strongly depend on temperature, the types of temperature dependence being highly diverse [139]. For example, the value of $|R_H|$ in Al–Cu–Fe and Al–Cu–Ru specimens with $R_H < 0$ is two orders of magnitude higher than typical values for metallic glasses and corresponds to an effective concentration n_{eff} of carriers on the order of $(2-5) \times 10^{20}$ cm^{-3} [152, 153]. The absolute value and sign of the Hall coefficient of icosahedral Al–Cu–Fe phases are essentially dependent on the chemical composition [154]. At low temperatures, the values of the Hall coefficient and electrical conductivity show correlation with the iron content. At an iron content of 12.5 at.%, R_H changes sign and σ falls to a minimum. The Hall coefficient for icosahedral Al–Re–Pd phases is positive at low temperatures, its absolute value is three orders of magnitude higher than characteristic $|R_H|$ values for amorphous metals [155], and its sign may change with a rise in temperature, depending on chemical composition. In icosahedral Y–Mg–Zn phases, $R_H < 0$ and the effective carrier concentration $n_{eff} \approx 2.3 \times 10^{21}$ cm^{-3}, which roughly corresponds to one carrier per 25 atoms [156]. The Seebeck coefficient of quasicrystal phases with low electrical conductivity, such as Al–Cu–Ru, shows a strong temperature dependence and sometimes changes sign [153]. In the Al–Re–Pd phase, it grows rapidly with the growing content of transition metals (palladium or rhenium) [157, 158]. In icosahedral phases with relatively high electrical conduction, e.g., R–Mg–Zn (R = Y, Dy, Tb, Ho, Er), the coefficient S linearly depends on temperature above approximately 50 K with the $S(T)$-curve slope between 0.015 and 0.030 μV K^{-2} [159]. Taken together, such intricate behavior of Hall and Seebeck coefficients of icosahedral phases points to an important role for the band structure.

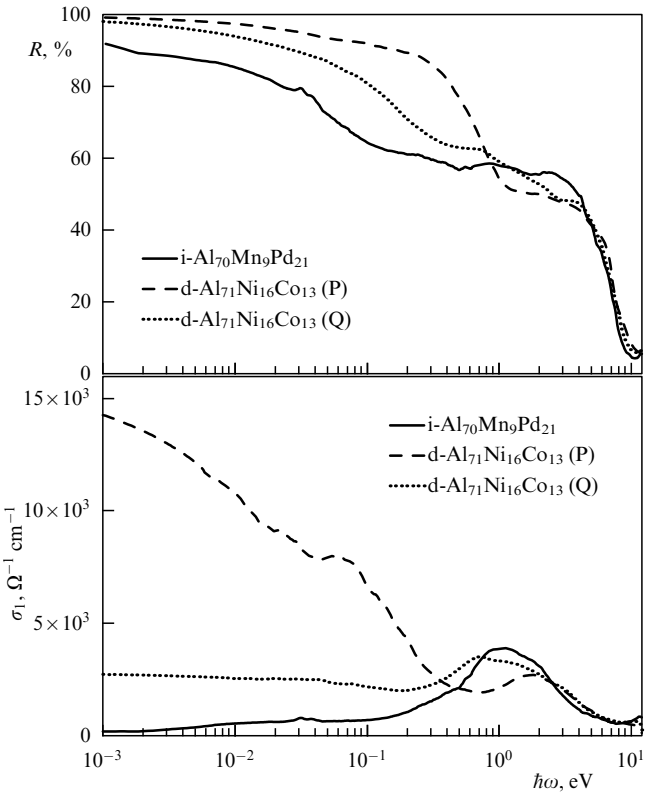

Figure 10. Reflection coefficient R and the real part $\sigma_1(\omega)$ of complex optical conductivity $\sigma(\omega)$ of the icosahedral $Al_{70}Mn_9Pd_{21}$ phase and decagonal $Al_{71}Ni_{16}Co_{13}$ phase for periodic direction (P) and quasiperiodic plane (Q) (taken from Ref. [166]).

5.2 Optical properties

The optical properties of quasicrystals differ from those of metals and semiconductors [160–163, 156]. In the low-frequency limit, reflection coefficient R of icosahedral phases is close to unity, and a characteristic feature of the real part $\sigma_1(\omega)$ of complex optical conductivity $\sigma(\omega)$ is the presence of a strong absorption band in the visible region of the spectrum (Fig. 10). It is believed that this band is related to excitations via a pseudogap in the excitation spectrum that opens after stabilization of the icosahedral phase by the Hume–Rothery mechanism. Another broad absorption band in the $\sigma_1(\omega)$ spectrum, attributable to bound state distribution, occurs in the middle and far IR regions. The Drude peak observed in $\sigma_1(\omega)$ spectra of both periodically ordered metals and disordered alloys is poorly discernable and practically unresolvable in the far IR region of optical conductivity spectra of icosahedral quasicrystals. A consistent description of optical conductivity spectra of icosahedral quasicrystals is possible in the framework of the Fermi multicomponent surface model. For example, optical conductivity spectra of the icosahedral Al–Pd–Re phase exhibit enhancement of σ_1 with temperature in the low-frequency region [164], which qualitatively agrees with the tenets of the model.

The optical conductivity spectra $\sigma_1(\omega)$ of decagonal phases are essentially anisotropic [165, 166]. For example, the main contribution to $\sigma_1(\omega)$ at low frequencies for the periodic direction of the decagonal Al–Ni–Co phase is provided by the narrow Drude peak with plasma frequency

$\omega_p \sim 1.2$ eV, free carrier scattering rate $\Gamma \sim 1.4 \times 10^{-2}$ eV, and two additional absorption bands at 0.1 and 2 eV in the higher-frequency region (Fig. 10). The optical conductivity $\sigma_1(\omega)$ of this material along the quasiperiodic plane is characterized by a much broader Drude peak with $\omega_p \sim 2$ eV, $\Gamma \sim 0.2$ eV, and a single high-frequency absorption band at 1 eV. It is supposed that absorption bands at 2 and 1 eV for the periodic direction and the direction in the quasiperiodic plane, respectively, are related to excitations via the pseudogap in the excitation spectrum. These bands are less apparent in the optical conductivity spectra of decagonal quasicrystals than in $\sigma_1(\omega)$ spectra of icosahedral quasicrystals due to the greater low-frequency conductivity of decagonal phases.

5.3 Superconductivity

Most quasicrystals are not superconductors, and the phases found to exhibit superconductivity in experiment are not ranked among those with perfect structure. Certain rational approximants of quasicrystals and their amorphous composition analogs can pass into the superconducting state. The cause behind the lack of superconductivity in perfect quasicrystals is the smallness of the electron–phonon coupling constant. Indeed, there is a dense set of reciprocal lattice vectors for a quasicrystal, and each scattering vector represents the reciprocal lattice vector. At the same time, the matrix element of electron–phonon interaction for the Umklapp processes is zero-valued.

In what follows, the most important results of research on superconductivity in quasicrystals will be discussed. Wong et al. [168] compared the electrical transport properties of $Al_{52.4}Cu_{12.6}Mg_{35}$ samples with Frank–Kasper type icosahedral and cubic structures and observed their transition to the superconducting state at 0.81 and 0.73 K, respectively. Temperature derivatives of the upper critical field H_{c2} at $T = T_c$, obtained from the measurement of the temperature dependence $H_{c2}(T)$, proved very similar (-3.3 and -2.7 kOe K^{-1} for icosahedral and cubic phases, respectively). Renormalized density of electronic states at the Fermi level calculated from $(dH_{c2}/dT)_{T_c}$ and electrical resistivity in the normal state for the icosahedral $Al_{52.4}Cu_{12.6}Mg_{35}$ phase is close to the density of states in the free-electron model.

Graebner and Chen [169] studied low-temperature specific heat and found that the cubic, icosahedral, and amorphous $Mg_3Zn_3Al_2$ phases obtained by the rapid quenching technique of the melt followed by thermal annealing change to the superconducting state at 0.31, 0.41, and 0.75 K, respectively. It was shown that the icosahedral $Mg_3Zn_3Al_2$ phase is a superconductor well described by the BCS theory in the weak-coupling limit with the density of electronic states at the Fermi level close to that in the free-electron model, and Debye temperature θ_D similar to that of the cubic phase. The icosahedral $Mg_3Zn_3Al_2$ phase proved to be in all respects much more akin to the crystalline cubic phase than to the amorphous one. Interestingly, the data on the temperature dependence of specific heat $C_s(T)$ in the superconducting state obtained in Ref. [169] do not give direct evidence of a linear-in-temperature contribution to low-temperature specific heat for $T < T_c$, which is associated with excitations of two-well tunneling systems responsible for the thermal and elastic properties of amorphous solids at low temperatures. Nevertheless, the data on specific heat $C_s(T)$ of the icosahedral $Mg_3Zn_3Al_2$ phase down to temperatures around 0.05 K, i.e., much below the critical temperature, permitted determining the upper limit of 0.55 μJ g^{-1} K^{-2} for the coefficient of the linear-in-temperature contribution to specific heat for $T < T_c$; this limiting value constitutes approximately half the respective coefficient for superconducting metallic $Zr_{70}Pd_{30}$ glass [170].

Stadnik et al. [171] investigated the electrical transport properties of the $Zr_{65}Al_{7.5}Ni_{10}Cu_{7.3}Fe_{0.2}Al_{10}$ alloy. Amorphous samples of this alloy obtained by rapid quenching were shown to change to the superconducting state at 1.7 K. Annealing of amorphous specimens gave rise to forming approximately 3×10^2 Å in size isometric inclusions of the icosahedral phase in the amorphous matrix which occupied more than 50% of the sample volume. Two-phase specimens failed to pass into the superconducting state, at least for $T > 1.5$ K; this means that inclusions of the icosahedral phase in the normal state suppress the critical temperature. Bearing in mind that the critical temperature of the icosahedral $Mg_3Zn_3Al_2$ phase is almost twice as low as that of alloys of identical composition in the amorphous state, it would be of interest to extend the temperature range of research on the electrical transport properties of two-phase $Zr_{65}Al_{7.5}Ni_{10}Cu_{7.3}Fe_{0.2}Al_{10}$ samples toward lower values.

The superconductivity of Ti–Zr–Ni alloys containing icosahedral phases was discussed in Refs [172, 173]. Resistivity measurements on samples of starting composition $Ti_{41.5}Zr_{41.5}Ni_{17}$ obtained by the rapid quenching technique in Ref. [173] were performed in a zero external magnetic field within a temperature range from 0.3 to 300 K, as well as at fixed field strengths of 0–16 kOe and temperatures 0.3–2 K. The authors concluded from their experimental findings that superconductivity may arise in this material at $T_c \approx 1.6$ K. Resistivity $\rho(T)$ of the Ti–Zr–Ni samples dropped stepwise below the values corresponding to the normal state as temperature decreased to less than 1.6 K. Zero resistance was recorded in a single specimen at $T \approx 0.35$ K. Because the samples of interest contained two different icosahedral phases and a third one with composition lying in the homogeneity region of the rational periodic 1/1 approximant, consistent analysis of the $\rho(T, H)$ data obtained in the above experiment encounters difficulty. Nevertheless, it is worth noting that temperature dependence of the upper critical field $H_{c2}(T)$ in the Ti–Zr–Ni phase with the maximum temperature of transition to the superconducting state determined from the initial deflection of the $\rho(T)$ curve from the level corresponding to the normal state gives a $-(dH_{c2}/dT)_{T_c}$ value on the order of 10 kOe K^{-1}. For comparison, $-(dH_{c2}/dT)_{T_c}$ values for amorphous $(Ti_xZr_{1-x})_{0.78}Ni_{0.22}$ superconductors, $0.1 \leqslant x \leqslant 0.3$, with transition temperatures in the range of 2.8–3.3 K fall within the range between 31 and 36 kOe K^{-1} [174].

5.4 Magnetism

Different types of magnetic behavior have been documented in quasicrystals, from diamagnetism [175–177] to spin-glass type freezing of magnetic moments [178–180], and even to ferromagnetic ordering [181–184]. The temperature dependence of magnetic susceptibility can be represented as the sum of diamagnetic contribution and paramagnetic contribution varying with temperature in accordance with the Curie–Weiss law [185] or the contribution from the spin-glass state [180]. Various contributions to magnetic susceptibility of icosahedral quasicrystals, including paramagnetic, Pauli spin, and

diamagnetic, were analyzed in Ref. [151], where it was shown that relatively weak diamagnetism is due to the atom-like diamagnetic contribution of conduction electrons in electron pockets of the multicomponent Fermi surface, while the Landau–Peierls type diamagnetic contribution is insignificant because electron effective mass is not small. At temperatures above Debye temperature θ_D, the Pauli paramagnetic contribution prevails; its temperature dependence is related to the pseudogap in the density of electronic states at the Fermi level.

Spin-glass type behavior is intrinsic — that is, impurity-unrelated in thermodynamically stable icosahedral quasicrystals, such as Al–Mn–Pd, R–Mg–Zn (R = Gd, Dy, Tb, Ho, Er), and R–Mg–Cd (R = Gd, Dy, Tb) phases. A distinctive feature of the spin-glass state in the icosahedral Al–Mn–Pd phase, suggested by magnetic and nuclear hyperfine contributions to low-temperature specific heat, is the unusually low concentration of magnetic moments involved in the freezing process. Such a concentration roughly corresponds to 1% of all Mn ions, suggesting the presence of their two types — magnetic and nonmagnetic ions [178]. Their origin is the subject of extensive experimental and theoretical research [186–188]. To recall, all Mn ions in canonical spin glasses $Cu_{1-x}Mn_x$, $Ag_{1-x}Mn_x$, and $Au_{1-x}Mn_x$ are magnetic. Also, it should be noted that both the fraction of such ions and the freezing temperature T_f of spin glass in icosahedral phases of the ternary Al–Mn–Pd system rapidly increase with increasing Mn concentration in the samples [189]. For example, the freezing temperature T_f increases sevenfold, from 0.5 to 3.5 K, upon a rise in Mn content from 9 to 11 at.% [178, 190]. For the icosahedral Al–Mn–Pd phase, the ratio of freezing temperature T_f to concentration x of magnetic ions, characterizing the interaction between magnetic moments, amounts to 450 K, i.e., comes up to the T_f/x ratio in canonical spin glasses $Cu_{1-x}Mn_x$, $Ag_{1-x}Mn_x$, and $Au_{1-x}Mn_x$ characterized by strong Ruderman–Kittel–Kasuya–Yosida exchange interaction between manganese magnetic moments [191, 192].

The spin-glass state was also revealed in the decagonal phase of a ternary Al–Mn–Pd system having a narrow homogeneity region near the $Al_{69.8}Mn_{18.1}Pd_{12.1}$ composition and containing twice as much Mn as the corresponding icosahedral phase [193, 194]. Third-order magnetic susceptibility of this phase has a minimum at freezing temperature $T_f = 12$ K, characteristic of spin glasses, while 'thermoremanent' magnetization M_{TR} at temperatures below T_f changes slowly with time following the power law, as is also typical of spin glasses. The temperature dependence of magnetic entropy of the decagonal $Al_{69.8}Mn_{18.1}Pd_{12.1}$ phase, related to magnetic moment freezing, suggests that a large part of Mn ions, similar to the icosahedral Al–Mn–Pd phase, have no magnetic moments at low temperatures. M Satoh and coworkers estimated the fraction of magnetic Mn ions in the decagonal Al–Mn–Pd phase at 14%, based on the results of magnetic measurements [193]. At the same time, NMR studies point to the fact that 50% of the Mn ions are magnetic [195]. Thus, the ratio of freezing temperature to concentration of magnetic ions, T_f/x, varies from 130 to 430 K, giving evidence of strong exchange interaction in the systems of interest.

The magnetic properties of R–Mg–Zn (R = Gd, Dy, Tb, Ho, Er) quasicrystals with the face-centered icosahedral structure are essentially different from those of icosahedral and decagonal phases of the ternary Al–Mn–Pd system first

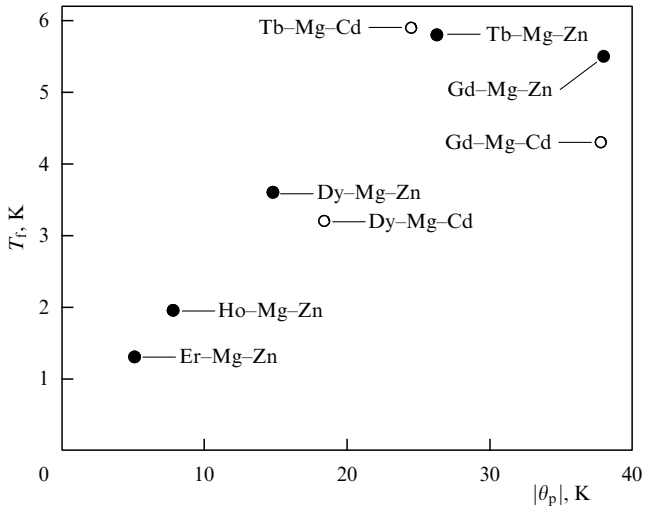

Figure 11. Dependence of freezing temperature T_f on absolute Curie paramagnetic temperature $|\theta_p|$ for icosahedral Gd–Mg–Zn [179], R–Mg–Zn (R = Dy, Tb, Ho, Er) [180], and R–Mg–Cd (R = Gd, Dy, Tb) [196] phases.

and foremost in that all ions of heavy rare-earth elements are magnetic, while interaction between them is weaker and characterized by T_f/x values lying within 15–70 K [180]. The process of magnetic moment freezing in icosahedral R–Mg–Zn quasicrystals is rather unusual. Crystal electric field effects account for marked local magnetic anisotropy in rare-earth Dy, Tb, Ho, and Er ions with nonzero angular momentum L [180, 156]. Local anisotropy can manifest itself as higher freezing temperature T_f of the icosahedral Tb–Mg–Zn phase compared with that of Gd–Mg–Zn despite the fact that the de Jennes parameter $\xi = (g-1)^2 J(J+1)$ for Tb is smaller than for Gd (Fig. 11). A similar relationship between freezing temperatures was documented for quasicrystalline phases with a primitive icosahedral structure (Tb–Mg–Cd and Gd–Mg–Cd) [196]. Thus, the process of magnetic moment freezing in icosahedral R–Mg–Zn and R–Mg–Cd quasicrystals resembles the behavior of axial spin glasses $Y_{1-x}R_x$ and $Sc_{1-x}R_x$ with the hexagonal structure [197].

An interesting feature of the low-temperature state of icosahedral R–Mg–Zn phases is short-range antiferromagnetic spin correlations between Ho^{3+} ion moments in Ho–Mg–Zn quasicrystals [198]. Equally unusual is the behavior of thermoremanent magnetization M_{TR} of icosahedral Tb–Mg–Zn quasicrystals, which grows linearly with the magnetic field H_{FC}, in which the sample of interest is cooled to the temperature at which the measurement is performed; such a behavior of $M_{TR}(H_{FC})$ is characteristic of superparamagnets but not spin glasses [199].

Icosahedral R–Mg–Zn phases are given very much attention in the light of discussion concerning the quasiperiodic magnetic long-range order of the antiferromagnetic type [200]. In earlier experiments with polycrystalline specimens, Hattori et al. [179], and Charrier and Schmitt [201] demonstrated that $R_8Mg_{42}Zn_{50}$ (R = Gd, Dy, Tb, Ho, Er) phases pass into the spin-glass state with freezing temperatures below 10 K, and their magnetic susceptibility in a wide temperature range above T_f can be described by the Curie–Weiss law with negative paramagnetic Curie temperature θ_p suggesting antiferromagnetic exchange interaction between moments of rare-earth ions. Charrier et al. [202] published powder

neutron-diffraction data obtained on polycrystalline samples, pointing to the possibility of transition of quasicrystals with $R = \mathrm{Tb}$, Dy, Ho, Er into the ground state with the antiferromagnetic long-range order of the quasiperiodic type for temperatures $T_\mathrm{N} > T_\mathrm{f}$. Worthy of note is the low intensity of lines corresponding to Bragg reflections, interpreted in Ref. [202] as manifestations of antiferromagnetic ordering; the neutronograms showed well-apparent diffuse magnetic scattering. In a later study, Islam et al. [203] measured neutron scattering in icosahedral $R-\mathrm{Mg}-\mathrm{Zn}$ phases, but failed to demonstrate signs of antiferromagnetic ordering in single-crystal powder samples. At the same time, some of the additional magnetic lines observed in paper [202] were reproduced in polycrystal specimens obtained by rapid cooling technique. Bearing in mind the currently available data from equilibrium phase diagrams of ternary $R-\mathrm{Mg}-\mathrm{Zn}$ systems in the concentration region corresponding to icosahedral phases, it is generally believed that the additional magnetic lines on neutronograms of polycrystalline samples could be related to the magnetic ordering of small inclusions of the periodically ordered phase. Therefore, the existence of antiferromagnetic ordering in quasicrystals is yet to be shown.

Ferromagnetic properties were revealed in various icosahedral phases including $\mathrm{Al}_{70-x}\mathrm{Pd}_{15}\mathrm{Mn}_{15}\mathrm{B}_x$ ($3 < x < 6$) and $\mathrm{Al}_{70-x}\mathrm{B}_x\mathrm{Pd}_{30-x}\mathrm{Fe}_y$ ($5 < x < 10$, $10 < y < 20$). The Curie temperature of $\mathrm{Al}_{70-x}\mathrm{Pd}_{15}\mathrm{Mn}_{15}\mathrm{B}_x$ quasicrystals falls between 480 and 550 K [181, 182]. The icosahedral $\mathrm{Al}_{70-x}\mathrm{B}_x\mathrm{Pd}_{30-y}\mathrm{Fe}_y$ phase is characterized by a Curie temperature from 280 to 340 K, maximum saturation magnetization $M_\mathrm{s} \approx 7.5$ G cm^3 g^{-1}, and mean hyperfine magnetic field $\langle H_\mathrm{hf}\rangle \approx 10^2$ kOe [183, 184]. Ferromagnetism in this phase is spatially nonuniform. Measurements of the Mössbauer effect showed that only 12–15% of the iron atoms in this phase have a magnetic moment. The magnetic properties of the icosahedral $\mathrm{Al}_{70-x}\mathrm{B}_x\mathrm{Pd}_{30-y}\mathrm{Fe}_y$ phase suggest the existence of large magnetic clusters $(2-3)\times 10^2$ Å in size. Such clusters contain around 4×10^4 rhombohedrons making up the Ammann–Mackay network.

Group-theoretical analysis shows that ferromagnetism is incompatible with icosahedral symmetry [204]. When a magnetic field is directed along the 5-, 3-, and 2-fold axes, icosahedral symmetry reduces to pentagonal, trigonal, and rhombic, respectively. The resulting magnetostriction must lead via phason distortions to a magnetically inhomogeneous state as confirmed by the published experimental data on ferromagnetism in quasicrystals with icosahedral ordering.

5.5 Thermal conduction

Thermal conduction in solids including quasicrystals is determined in a broad range by lattice and electron contributions. Due to the relatively low density of carriers, the dominant thermal conduction mechanism in typical icosahedral quasicrystals for $T \lesssim 100$ K is heat transfer by excitations of the quasicrystal lattice. The behavior of the temperature dependence of lattice thermal conductivity $\lambda_\mathrm{l}(T)$ of icosahedral crystals differs from that of both periodically ordered crystals and amorphous solids.

Curve $\lambda_\mathrm{l}(T)$ for periodic crystals shows a well-apparent maximum, as a rule in the temperature range from 10 to 30 K. In periodic crystals and a temperature range somewhat above the maximum in $\lambda_\mathrm{l}(T)$, the heat resistance of the lattice is determined by the Umklapp processes and therefore grows exponentially with temperature due to the exponentially

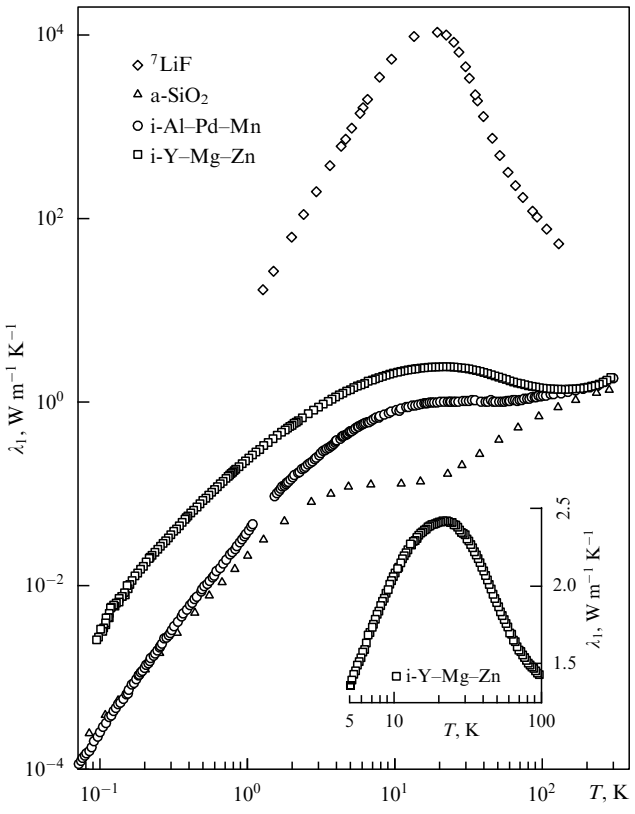

Figure 12. Lattice thermal conductivity λ_l of icosahedral Al–Mn–Pd and Y–Mg–Zn phases as a function of temperature [213, 214, 159]; heat conductivities of a periodically ordered ^{7}LiF crystal and amorphous silicon dioxide are shown for comparison (taken from Refs [206, 208]); the inset depicts the $\lambda_\mathrm{l}(T)$ dependence for the icosahedral Y–Mg–Zn phase near the maximum.

increasing number of occupied high-frequency phonon states for which such processes are permitted [205]. It should be recalled that the experimental verification of the regime in which Umklapp processes are responsible for heat resistivity $\lambda_\mathrm{l}^{-1}(T)$ by examining the dependence $\lambda_\mathrm{l}(T) \propto T^\xi \times \exp(\theta_\mathrm{D}/bT)$, where ξ and b are on the order of unity, is nontrivial in character. Such dependence $\lambda_\mathrm{l}(T)$ can be observed in a restricted temperature range of $1/30 \lesssim T/\theta_\mathrm{D} \lesssim 1/10$ using isotopically pure single crystals of high structural quality [206]. Transition (upon a fall in temperature) to the heat conduction regime limited by phonon scattering on sample boundaries (Casimir regime) or conduction electrons in dielectric and metallic crystals, respectively, accounts for a maximum of phonon thermal conductivity dependence on the temperature, as shown in Fig. 12 for ^{7}LiF [207].

Lattice thermal conductivity λ_l of amorphous solids grows monotonically with temperature and reaches the so-called λ-plateau in a range between 2 and 10 K. Figure 12 illustrates such behavior of the $\lambda_\mathrm{l}(T)$ curve for amorphous silicon dioxide [208]. For $T \lesssim 1$ K, lattice thermal conductivity of amorphous solids varies with temperature according to the power law $\lambda_\mathrm{l}(T) = AT^n$, with exponent n close to 2 due to low-frequency excitations, the spectral density of which in a wide frequency range shows but weak frequency dependence. These excitations fail to propagate or transfer heat. The scattering of mobile acoustic modes involving stationary low-frequency excitations restricts the mean free path l of

the acoustic modes and therefore lattice thermal conductivity λ_l. The low-temperature thermal and elastic properties of amorphous solids, related to low-frequency excitations, are described by the tunneling states model [209, 210]. It is supposed that the λ-plateau is due to a sharp decrease in the mean free path l of lattice excitations with increasing frequency ω [208]. The available experimental data indicate that $l \propto \omega^n$, where the exponent n ranges from -4 to -3 [211]. Above the λ-plateau, the lattice thermal conductivity of amorphous solids begins to grow with temperature, and λ_l becomes close to the so-called minimal conductivity λ_{min} corresponding to the regime in which the mean free path of lattice excitations equals one-half of the excitation wavelength [212].

Figure 12 illustrates the temperature dependence of lattice thermal conductivity $\lambda_l(T)$ of the icosahedral Al–Mn–Pd phase. Thermal conductivity at temperatures below 1 K is limited by phonon resonance scattering on low-frequency excitations described by the tunneling states model and varies roughly as T^2 [213–215]. The existence of two-well tunneling systems in Al–Mn–Pd quasicrystals was demonstrated in low-temperature ultrasonic experiments by Vernier et al. [216], who observed two characteristic signs of their presence, viz. a contribution to the temperature dependence of the transverse speed of sound $v_t(T)$ that is logarithmic in temperature and nonlinear absorption of transverse acoustic waves [217]. Scattering of lattice excitations on tunneling states as a rule reduces λ_l to values one order of magnitude lower than in the Casimir limit.

At temperatures above several dozen kelvins, lattice thermal conductivity slowly increases with temperature; in this temperature region, vibrational modes of the quasicrystal lattice responsible for heat transfer cannot be represented as propagating collective excitations. Below the high-temperature regime, the quasicrystal thermal conductivity curve exhibits two regions: one of them corresponds to phonon scattering on tunneling states in which $d\lambda_l/dT > 0$, and the other to Umklapp processes with $d\lambda_l/dT < 0$. The maximum separating these regions is much lower and wider than the peak between boundary scattering and Umklapp regions in the thermal conductivity curve of a periodically ordered crystal. In the case of strong phonon scattering from tunneling states, this maximum and the region of Umklapp processes can degenerate into a plateau ($d\lambda_l/dT \approx 0$).

Reduction of λ_l with growing temperature in the intermediate temperature range is due to Umklapp processes that have the following features in quasicrystals. Unlike periodically ordered crystals in which the natural scale of Umklapp processes is determined by the reciprocal lattice vector, vibrational excitation momentum in quasicrystals can be imparted to the lattice in small portions, the values of which are not bound from below. For this reason, the rate of Umklapp processes in quasicrystals shows a weaker, i.e., power-like, temperature dependence [120]. As a result, curve $\lambda_l(T)$ has a more slanting portion of negative slope $d\lambda_l/dT$ than in periodic crystals and even the λ-plateau that, however, lies at significantly higher temperatures than the λ-plateau of a typical amorphous material; this feature is shared by all quasicrystals. Accordingly, the maximum of the dependence $\lambda_l(T)$ reflects transition from the regime of dominant phonon scattering by tunneling states to the regime where Umklapp processes become the predominated mechanism of lattice thermal resistance. The above features of the $\lambda_l(T)$ curve for a quasicrystal, viz. the maximum or the λ-plateau, were described for temperature dependences of lattice thermal conduction of both icosahedral [213–218] and decagonal phases along the quasiperiodic plane [166, 219].

Electron contribution λ_{el} to thermal conductivity in icosahedral quasicrystals becomes significant at temperatures above 100 K, and in phases with a high carrier concentration, e.g., Y–Mg–Zn, even at lower temperatures. Estimations of the electronic contribution under the assumption of validity of the Wiedemann–Franz law applicable to the multicomponent Fermi surface model at high temperatures yield the dependence $\lambda_{el}(T)$ that is quadratic in temperature [150]. These estimates are confirmed by calculations of heat conductivity of the icosahedral Al–Cu–Fe phase based on the measurements of thermal diffusivity and specific heat at high temperatures: in the range from 300 to 800 K, where electronic heat conductivity is substantially higher than the lattice one, λ changes with temperature as T^α (where $\alpha = 1.9 \pm 0.1$), and the assumption of $\alpha = 2$ leads to the Lorentz number $L \approx 2.8 \times 10^{-8}$ W Ω K^{-2}, i.e., somewhat higher than the value of L_0 in the Sommerfeld model [220].

5.6 Mechanical and surface properties

There is a wealth of data available on the mechanical properties of quasicrystals. To begin with, they are nonplastic at temperatures below 600 °C. Polycrystal samples undergo destruction along the grain boundaries. They become plastic at temperatures above 650 °C, when destruction occurs inside the grains. As is known, plasticity is a function of dislocation mobility. In quasicrystals, the Burgers dislocation vector contains a phason component; in other words, dislocation movements are limited by diffusion that is weak for $T \leqslant 600$ °C; it accounts for the poor dislocation mobility in quasicrystals. It is not the sole manifestation of aperiodic long-range order. The elastic moduli of quasicrystals and ordinary crystals being roughly equal, their yield points are very close, too. However, the growing strain in periodic crystals results in their cold hardening, whereas quasicrystals undergo strain weakening under the same conditions [221]. This effect is related to aperiodic long-range order and can be explained by the fact that the strain results in violation of the structural correspondence rule above and beneath dislocation glide planes due to phason distortions; this leads eventually to weakening. Creep also has peculiarities; namely, the low-stress creep rate decreases, and the high-stress one increases. Other characteristics (microhardness, etc.) also reflect the influence of the aperiodic long-range order.

Quasiperiodicity is maintained on clean surfaces, too. Similar to ordinary periodically ordered crystals, such surfaces are formed by flat grains separated by steep steps [221]. The surface of Al-based quasicrystals is enriched in aluminium. Quasicrystals are characterized by low surface tension, intermediate between that of teflon and stainless steel. The surface energy of perfect quasicrystals is 25% higher than in teflon. The low surface energy is due to the presence of a pseudogap in the electronic spectrum; in Al-based quasicrystals, it is attributable to the small contribution from Al electronic 3p-states to the density of states; hence, the low friction coefficient equaling roughly 0.12–0.14 for the icosahedral Al–Cu–Fe phase. The nature of small friction coefficient is attributable to the specific properties of chemical bonds (largely covalent) near the surface. A small addition (about 5%) of the cubic β-AlFe(Cu) phase to the quasicrystalline $Al_{62}Cu_{25.5}Fe_{12.5}$ alloy doubles its friction

coefficient. In the atmosphere of oxygen, Al-containing quasicrystals undergo passivation and form a thin protective layer of aluminium oxide. Strong oxidation may result in restructuring of the surface and its change to the crystalline state. Inasmuch as the diffusion coefficients of quasicrystal constituent elements are lower than in pure elements, it is the surface layer that governs which element undergoes oxidation. At high temperatures, the oxidation rate of the Al – Cu – Fe surface increases, the copper content changes, and copper initiates a transition of θ-Al_2O_3 to α-Al_2O_3. In other words, corrosion resistance of the quasicrystalline alloy is largely due to oxidation of the constituent elements rather than to its quasicrystalline nature, per se.

6. Practical applications

Interest in the practical applications of quasicrystals first and foremost arises from the unusual combination of their high hardness, corrosion and wear resistances with low heat conductivity, 'wettability', and small friction coefficient. The use of quasicrystalline phases of single- and polycrystals as construction materials is limited by their high fragility and poor deformability at room temperature. This limitation is possible to obviate by using quasicrystalline phases in the form of coatings, inclusions in two-phase materials, or fillers in composite materials.

Coverings based on the icosahedral Al – Cu – Fe phase are readily compatible with aluminium alloys, stainless steel, and cast iron; they show high wear and corrosion resistances, and high-temperature stability. Their combination with cheap starting materials and simple coating techniques opens up good prospects for future applications in the chemical industry. At present, the Sitram company (France) produces a variety of cooking utensils with Cybernox nonstick coatings containing the Cr-doped icosahedral Al – Cu – Fe phase.

The inclusions of quasicrystal phases in such matrices as steel, aluminium, and Zr- and Mg-based alloys improve their strength and plasticity, especially at high temperatures. It is possible to produce such two-phase materials, for instance, by the crystallization of respective many-component melts in a specified region of the equilibrium phase diagram. Sandvik Bioline IRK91 maraging steel proved to be the first material comprising quasicrystalline inclusions that found industrial application. It contains, besides Fe, 12 wt.% Cr, 9 wt.% Ni, 4 wt.% Mo, 2 wt.% Cu, 0.9 wt.% Ti, 0.3 wt.% Al, 0.15 wt.% Si, and less than 0.05 wt.% C and N [222, 223]. After hardening, this steel acquires the martensite structure with high dislocation density and contains practically no inclusions of other phases. Aging leads to formation in the martensite matrix of particles of the thermodynamically stable icosahedral phase having the following composition: 50 wt.% Mo, 30 wt.% Fe, 15 wt.% Cr, and trace amounts of Ni and Si [222, 232]. The maximum hardness of Sandvik Bioline IRK91 steel after thermal treatment is estimated (by the Vickers method) at 730 HV, and its breaking strength amounts to 3000 MPa. This steel is the best material for superfine suture needles with an inner canal used in eye microsurgery.

Worthy of note among multiphase materials containing inclusions of icosahedral quasicrystals are aluminium-based Al – Mn – Ce – Co and Al – Cr – Ce – Co alloys obtained by extrusion. They have a breaking strength of 500 – 850 MPa, Young's module on the order of 100 GPa, a relative extension 6–25%, an impact strength of 60 – 180 kJ m^{-2}, and good ductility [224]. At 200 °C, their strength amounts to 200 MPa, which is much higher than in aluminium alloys strengthened by aging. Taken together, these properties characterize such materials as a new class of high-strength aluminium-based alloys.

A promising field for application of quasicrystals is the transformation of solar energy. The possibility of using them in selective absorbers of solar radiation utilized to heat water in thermal electric generators and domestic water heaters is based on the specific features of their light reflection spectra in visible and IR regions. The spectra of quasicrystals with an icosahedral structure have strong absorption bands in the visible region and their reflection coefficients in the IR region are high, which allows thermal radiation loss to be reduced to a minimum.

Much attention has recently been given to photon quasicrystals, i.e., artificial heterostructures being aperiodic analogs of crystalline photon crystals (transparent objects with a periodically modulated refraction index). Diffraction gives rise to the so-called photon band gap, i.e., a frequency interval with markedly reduced transparency, in the energy spectrum of electromagnetic radiation spreading in such structures. A significant reduction in radiation intensity occurs in the case of a sufficiently high depth of refraction index modulation, e.g., when the modulation period is roughly equal to the radiation wavelength. In periodically modulated structures, the band gap is anisotropic and depends on the directions of propagation and polarization of electromagnetic waves. In quasicrystal structures, such as those having octagonal or pentagonal symmetry, the band gap is more isotropic and the reduction in transparency is independent of the propagation direction due to well-apparent point symmetry and aperiodic long-range order. Photon quasicrystals already find application in electronics [225]. Phonon quasicrystals (artificial structures with quasi-periodic modulation of acoustic impedance) are also being extensively investigated as candidate materials for acoustic filters, mirrors, and acoustic baffles [225].

Other promising fields for practical applications of quasicrystals and materials containing them is the manufacture of catalysts, thermoelectric refrigerators and generators, metal hydride hydrogen storage systems, and quasicrystal superlattices for the generation of higher harmonics in laser devices.

7. Conclusions

The present review is devoted to the peculiarities in the structure and properties of quasicrystals. Naturally, it does not cover all issues pertinent to this topic. We did not discuss experiments on studying local atomic structure by X-ray absorption spectroscopy techniques with the use of synchrotron sources, atomic-resolution electron microscopy, tunneling experiments, NMR studies, or the Mössbauer effect. Despite the current emphasis on traditional materials science, quasicrystals remain objects of practical and academic interest. While their structure is being studied fairly well and can be simulated by a variety of well-developed and experimentally verified models, the properties are still a matter of controversy, giving rise to much speculation. Moreover, most experiments have been performed at low or relatively low (below room) temperatures, whereas the high-temperature range up to melting and peritectic decomposition temperatures remains virtually unexplored, although it is here

that the most interesting effects can be expected to occur. The contribution of electrons to electrical conduction and heat conduction increases at elevated temperatures above the Debye temperature θ_D and fulfillment of the Wiedemann–Franz law can be confirmed experimentally. Optical studies may reveal Drude peaks in optical conductivity and high light reflection coefficients in the visible part of the spectrum. New specific heat effects are likely to be discovered at elevated temperatures. An additional electronic contribution to specific heat can be anticipated at temperatures higher than the Debye temperature due to enhanced electron–phonon scattering; the same refers to contributions related to phason dynamics. All these effects require experimental verification. Equally interesting is the problem of the temperature-dependent behavior of static electrical conductivity. For example, transition to the variable-range-hopping conductivity regime at low temperatures is observed only in polycrystal specimens of the icosahedral Al–Pd–Re phase with $R > 10$, whereas Al–Pd–Re single crystals and other icosahedral phases fail to exhibit such a regime. Polycrystalline samples of the icosahedral Al–Pd–Re phase behave like granular electronic systems in which tunneling and the Coulomb blockade are the main factors responsible for electrical conduction.

Creation of artificial quasicrystal structures, viz. heterojunctions, photon quasicrystals, and quasicrystalline sequences of quantum wells, is a rapidly developing research field. Photon quasicrystals are more convenient for practical applications than their periodic analogs by virtue of the presence of isotropic photon band gap. The spectra of one- and two-particle excitations in quasicrystalline sequences of quantum wells are beginning to attract the attention of theorists [226]. These studies may reveal resonance passage in selected energy regions and localization of excitations at finite perturbations in one-dimensional structures. Liquid quasicrystals are equally interesting objects [227]. Finally, it is worth mentioning the recent discovery of the icosahedral Al–Cu–Fe phase inclusions in mineral agglomerations containing cupalit and khatyrkit from volcanic rocks of the Koryak Upland [228]. In a word, quasicrystals continue to interest theorists and experimentalists, despite the long history of previous research.

The authors are grateful to K Edagawa for permission to reproduce the electron diffraction patterns of the icosahedral $Al_{69.5}Pd_{21}Mn_{9.5}$ alloy. The work was supported by RFBR (grants 08-02-01461-a; 09-02-00147-a) and the Higher School Scientific Potential Development Program (2009–2010) being implemented under the auspices of the Russian Federation Ministry of Education and Science (grant RNP.2.1.1/1552). The authors are also thankful to the Goran Gustafsson foundation for nature sciences and medical research.

8. Appendices

8.1 The number τ

The number τ (golden ratio) represents a special class of irrational numbers called algebraic integers defined as roots of the algebraic equation

$$x^n + a_{n-1}x^{n-1} + \ldots + a_0 = 0\,,$$

where all a_n are integers. The number τ is defined as a solution to the simplest quadratic equation $\tau^2 = \tau + 1$ (self-similarity equation). Written in the form $1 = 1/\tau + 1/\tau^2$, it defines the division of a unit length segment into two pieces, $1/\tau$ and $1/\tau^2$ in size. Their proportional ratio is τ. The number τ can be represented as a continued fraction

$$\tau = \{1,1,1,\ldots\} \equiv 1 + \cfrac{1}{1 + \cfrac{1}{1 + \cfrac{1}{1 + \ldots}}}$$

and is the fixed point of a hyperbolic map. Related to the number τ is a sequence of Fibonacci numbers generated by the recurrent relation $F_{n+2} = F_{n+1} + F_n$ with initial conditions $F_0 = 1$, $F_1 = 1$. For large n, $F(n) = \tau^n/\sqrt{5}$, and $\lim_{n\to\infty} F_{n+1}/F_n = \tau$. Quasicrystals with 5- and 10-fold symmetries are self-similar with respect to stretching by a factor of τ. Quasicrystals with 8th and 12th orders of symmetry have self-similarity stretching factors $(1+\sqrt{2})/2$ and $(2+\sqrt{3})/2$, respectively. It should be emphasized that self-similarity is a peculiar symmetry of a system with respect to uniform stretching of its dimensions (scale invariance or scaling). Self-similarity of both quasicrystals and crystals implies the existence of such points in a space that stretching by a factor of q toward them converts a lattice into itself.

8.2 Incommensurate and long-period structures

The periodicity of a crystal manifests itself in the periodicity of its diffraction patterns. The diffraction pattern of incommensurate and long-period structures is characterized by satellite reflections. Imagine a periodic structure with sites $x_n = an$, where a is the interatomic distance, and n is an integer. Displacement of atoms to new positions

$$X_n = x_n + f\sin(qxn)\,, \quad q = q_1\left(\frac{2\pi}{a}\right) \tag{A.1}$$

modulates the structure. If q_1 is a nonzero rational number, the structure (A.1) is also periodic but has large unit cells (a commensurate long-period structure). When q_1 is an irrational number, the structure is an incommensurate one lacking periodicity but remaining quasiperiodic (the quasiperiodic function being a superposition of periodic functions with mutually incommensurate periods). The term 'quasiperiodicity' is borrowed from the theory of dynamical systems: a system is quasiperiodic in time if it is described by the superposition of several incommensurate frequencies. The incommensurability may be caused not only by atomic displacements; it may just as well arise from magnetic modulation (in compounds containing rare-earth elements, compositional inhomogeneities in nonstoichiometric structures, rare-earth metals with ordered magnetic moments), and compositional inhomogeneities in nonstoichiometric structures. The structure of incommensurate phases is convenient to describe applying the apparatus of multidimensional crystallography, which was later employed in studying quasicrystals. For example, all diffraction peaks for an ordinary periodically modulated crystal are defined by three indices: $K = ha^* + kb^* + lc^*$, where a^*, b^*, c^* are basis vectors of the reciprocal lattice, and h, k, l are integers (Miller indices). In the case of modulation, the diffraction vector is given by

$$K = ha^* + kb^* + lc^* + m(\alpha a^* + \gamma c^*)\,.$$

Peaks with $m = 0$ are the main reflections, and those with $m \neq 0$ are satellite ones. In this case, there is no three-

dimensional basis for which a^*, b^*, c^* and $q = \alpha a^* + \gamma c^*$ are all integers. However, Bragg peaks can be regarded as a projection of Bragg peaks of a 4D reciprocal lattice onto three-dimensional space. Thus, K is the projection K_3 of the four-dimensional reciprocal lattice with integer coordinates h, k, l, m. These Bragg peaks correspond to a 4D periodic structure; the real physical structure is determined by the section of this four-dimensional periodic structure by a three-dimensional hyperplane. Accordingly, the hyperspace for 3D quasicrystals is six-dimensional, and diffraction vectors have the form

$$K = (h_1 + h_4\tau,\ h_2 + h_5\tau,\ h_3 + h_6\tau)\,.$$

References

1. Landau L D, Lifshitz E M *Statisticheskaya Fizika* (Statistical Physics) Pt. 1 (Moscow: Nauka, 1976) p. 440 [Translated into English (Oxford: Pergamon Press, 1980)]
2. Shechtman D et al. *Phys. Rev. Lett.* **53** 1951 (1984)
3. Levine D, Steinhardt P J *Phys. Rev. Lett.* **53** 2477 (1984)
4. Senechal M *Quasicrystals and Geometry* (Cambridge: Cambridge Univ. Press, 1996)
5. Schrödinger E *What is Life? The Physical Aspect of the Living Cell and Mind and Matter* (Cambridge: Univ. Press, 1967) [Translated into Russian (Moscow: Atomizdat, 1972)]
6. Kimura K et al. *J. Solid State Chem.* **133** 302 (1997)
7. Shoemaker D P, Shoemaker C B, in *Introduction to Quasicrystals* (Ed. M V Jarič) (Boston: Academic Press, 1988) p. 1
8. de Jongh L J (Ed.) *Physics and Chemistry of Metal Cluster Compounds* (Dordrecht: Kluwer Acad. Publ., 1994)
9. Bradley A J, Goldschmidt H J *J. Inst. Met.* **65** 403 (1939)
10. Prevarskii A P *Izv. Akad. Nauk SSSR Metally* (4) 220 (1971)
11. Tsai A-P, Inoue A, Masumoto T *Jpn. J. Appl. Phys.* **26** L1505 (1987)
12. Hardy H K, Silcock J M *J. Inst. Met.* **84** 423 (1955)
13. Dubost B et al. *Nature* **324** 48 (1986)
14. Sastry G V S et al. *Mater. Res. Bull.* **13** 1065 (1978)
15. Padezhnova E M et al. *Izv. Akad. Nauk SSSR Metally* (4) 204 (1982)
16. Luo Z et al. *Scripta Metall.* **28** 1513 (1993)
17. Janot C, Mosseri R (Eds) *Proc. of the 5th Intern. Conf. on Quasicrystals, 22 – 26 May 1995, Avignon, France* (Singapore: World Scientific, 1995)
18. Takeuchi S, Fujiwara T (Eds) *Proc. of the 6th Intern. Conf. on Quasicrystals, 26 – 30 May 1997, Tokyo, Japan* (Singapore: World Scientific, 1998)
19. "Proc. of the 7th Intern. Conf. on Quasicrystals, 20 – 24 September 1999, Stuttgart, Germany" *Mater. Sci. Eng. A* **294 – 296** (2000) pp. 1 – 912
20. "Proc. of the 8th Intern. Conf. on Quasicrystals, 8 – 13 September 2002, Bangalore, India" *J. Non-Cryst. Solids* **334 – 335** (2004)
21. "Proc. of the 9th Intern. Conf. on Quasicrystals, 22 – 26 May 2005, Ames, Iowa, USA" *Philos. Mag.* **86** (3 – 5); (6 – 8) (2006)
22. "Quasicrystals: the Silver Jubilee" *Philos. Mag.* **88** (13 – 15) (2008)
23. "Proc. of the 10th Intern. Conf. on Quasicrystals, 6 – 10 July 2008, Zürich, Switzerland" *Z. Kristallogr.* **223** (11 – 12) (2008); **224** (1 – 2) (2009)
24. Stadnik Z M (Ed.) *Physical Properties of Quasicrystals* (Berlin: Springer, 1999)
25. Trebin H-R (Ed.) *Quasicrystals: Structure and Physical Properties* (Weinheim: Wiley-VCH, 2003)
26. Suck J-B, Schreiber M, Häussler P (Eds) *Quasicrystals* (Berlin: Springer-Verlag, 2002)
27. Janssen T, Chapuis G, de Boissieu M *Aperiodic Crystals: From Modulated Phases to Quasicrystals* (Oxford: Oxford Univ. Press, 2007)
28. Fujiwara T, Ishii Y (Eds) *Quasicrystals* (Amsterdam: Elsevier Science, 2008)
29. Steurer W, Deloudi S *Crystallography of Quasicrystals* (New York: Springer, 2009)
30. Ritsch S, Ph.D. Thesis (Zürich: Eidgenössische Technische Hochschule, 1996)
31. Janot C, Dubois J M *J. Phys. F: Met. Phys.* **18** 2303 (1988)
32. Tsai A-P, Inoue A, Masumoto T *Jpn. J. Appl. Phys.* **27** L1587 (1988)
33. Guryan C A et al. *Phys. Rev. Lett.* **62** 2409 (1989)
34. Kimura K, Takeuchi S, in *Quasicrystals: The State of the Art* (Eds D P DiVincenzo, P J Steinhardt) (Singapore: World Scientific, 1991) p. 313
35. Tsai A-P et al. *Mater. Trans. JIM* **31** 98 (1990)
36. Beeli C, Nissen H-U, Robadey J *Philos. Mag. Lett.* **63** 87 (1991)
37. Beeli C, Ph.D. Thesis (Zürich: Eidgenössische Technische Hochschule, 1992)
38. Berenson R, Birman J L *Phys. Rev. B* **34** 8926 (1986)
39. Kycia S W et al. *Phys. Rev. B* **48** 3544 (1993)
40. Härtwig J et al. *J. Phys. D* **34** A103 (2001)
41. Drehman A J, Pelton A R, Noack M A *J. Mater. Res.* **1** 741 (1986)
42. Ramachandrarao P, Sastry G V S *Pramana* **25** L225 (1985)
43. Lilienfeld D A et al. *Phys. Rev. Lett.* **55** 1587 (1985)
44. Follstaedt D M, Knapp J A *J. Appl. Phys.* **59** 1756 (1986)
45. Cassada W A et al. *Phys. Rev. Lett.* **56** 2276 (1986)
46. Budai J D, Aziz M J *Phys. Rev. B* **33** 2876 (1986)
47. Chen H S, Kortan A R, Parsey J M (Jr.) *Phys. Rev. B* **36** 7681 (1987)
48. Guyot P, Kramer P, de Boissieu M *Rep. Prog. Phys.* **54** 1373 (1991)
49. Tsai A P, in *Physical Properties of Quasicrystals* (Ed. Z M Stadnik) (Berlin: Springer, 1999) p. 5
50. Fisher I R et al. *Mater. Sci. Eng. A* **294 – 296** 10 (2000)
51. Ranganathan S, Chattopadhyay K *Annu. Rev. Mater. Sci.* **21** 437 (1991)
52. McAlister A J et al. *Scripta Met.* **21** 103 (1987)
53. Elser V, Henley C L *Phys. Rev. Lett.* **55** 2883 (1985)
54. Henley C L, Elser V *Philos. Mag.* **53** 59 (1986)
55. Tsai A P, in *The Science of Complex Alloy Phases* (Eds P Turchi, T Massalski) (Pittsburgh: TMS Publ., 2005) p. 201
56. Goldman A I, Kelton R F *Rev. Mod. Phys.* **65** 213 (1993)
57. Koskenmaki D C, Chen H S, Rao K V *Phys. Rev. B* **33** 5328 (1986)
58. Chen H S et al. *Phys. Rev. B* **35** 9326 (1987)
59. Penrose R *Bull. Inst. Math. Appl.* **10** 266 (1974)
60. de Bruijn N G *Proc. K. Ned. Akad. Wet. A* **84** 39 (1981)
61. Levitov L S *Zh. Eksp. Teor. Fiz.* **93** 1832 (1987) [*Sov. Phys. JETP* **66** 1046 (1987)]
62. Gardner M *Sci. Am.* **236** (1) 110 (1977)
63. Kalugin P A, Kitaev A Yu, Levitov L S *Pis'ma Zh. Eksp. Teor. Fiz.* **41** 119 (1985) [*JETP Lett.* **41** 145 (1985)]
64. Kalugin P A, Kitayev A Yu, Levitov L S *J. Physique Lett.* **46** 601 (1985)
65. Gratias D, Cahn J W *Scripta Met.* **20** 1193 (1986)
66. Kramer P, Neri R *Acta Cryst. A* **40** 580 (1984)
67. de Wolff P M *Acta Cryst. A* **30** 777 (1974)
68. Janner A, Janssen T *Phys. Rev. B* **15** 643 (1977)
69. Elser V *Phys. Rev. B* **32** 4892 (1985)
70. Elser V *Acta Cryst. A* **42** 36 (1986)
71. Henley C L *Phys. Rev. B* **34** 797 (1986)
72. Kramer P *Acta Cryst. A* **43** 486 (1987)
73. Shelekhov E V, Skakov Yu A *Kristallografiya* **35** 1354 (1990)
74. Korepin V E *Zapiski Nauchn. Seminarov LOMI* **155** 116 (1986)
75. Stephens P W, Goldman A I *Phys. Rev. Lett.* **56** 1168 (1986)
76. Robertson J L, Moss S C *Phys. Rev. Lett.* **66** 353 (1991)
77. Chidambaram R et al., in *Quasicrystals and Incommensurate Structures in Condensed Matter* (Eds D Romeu, V Castano, A Gomez) (Singapore: World Scientific, 1990) p. 330
78. Manaila R et al. *J. Phys. Condens. Matter* **6** 2307 (1994)
79. Ishii Y *J. Non-Cryst. Solids* **117 – 118** 840 (1990)
80. Chidambaram R et al. *Phys. Rev. B* **48** 3030 (1993)
81. van Smaalen S, de Boer J L, Shen Y *Phys. Rev. B* **43** 929 (1991)
82. de Boissieu M, Janot C, Dubois J M *J. Phys. Condens. Matter* **2** 2499 (1990)
83. Audier M, Guyot P *Mater. Trans. JIM Suppl.* **29** 427 (1988)
84. Cahn J W, Gratias D, Mozer B *J. Physique* **49** 1225 (1988)
85. Gratias D, Cahn J W, Mozer B *Phys. Rev. B* **38** 1643 (1988)
86. Hiraga K et al. *Philos. Mag. B* **67** 193 (1993)
87. de Boissieu M et al. *Phys. Rev. Lett.* **72** 3538 (1994)
88. Yamaguchi T, Fujima N *J. Non-Cryst. Solids* **117 – 118** 765 (1990)
89. Rakshun Ya B, Cand.Sc. Thesis (Moscow: Moscow Engineering Physics Institute, 2007)
90. Gummelt P *Geometriae Dedicata* **62** 1 (1996)

91. Alexander S, McTague J *Phys. Rev. Lett.* **41** 702 (1978)
92. Mermin N D, Troian S M *Phys. Rev. Lett.* **54** 1524 (1985)
93. Smith A P, Ashcroft N W *Phys. Rev. B* **38** 12942 (1988)
94. Smith A P *Phys. Rev. B* **42** 1189 (1990)
95. Olenev D V, Korzhavyi P A, Vekilov Yu Kh *Zh. Eksp. Teor. Fiz.* **104** 4130 (1993) [*JETP* **77** 998 (1993)]
96. Olenev D V, Vekilov Yu Kh *Pis'ma Zh. Eksp. Teor. Fiz.* **60** 706 (1994) [*JETP Lett.* **60** 726 (1994)]
97. Kohmoto M, Kadanoff L P, Tang C *Phys. Rev. Lett.* **50** 1870 (1983)
98. Kohmoto M, Sutherland È, Tang C *Phys. Rev. B* **35** 1020 (1987)
99. Tsunetsugu H et al. *J. Phys. Soc. Jpn.* **55** 1420 (1986)
100. Tsunetsugu H et al. *Phys. Rev. B* **43** 8879 (1991)
101. Fujiwara T, in *Physical Properties of Quasicrystals* (Ed. Z M Stadnik) (Berlin: Springer, 1999) p. 169
102. Yamamoto S, Fujiwara T *Phys. Rev. B* **62** 8841 (1995)
103. Vekilov Yu Kh, Isaev E I, Arslanov S F *Phys. Rev. B* **62** 14040 (2000)
104. Vekilov Yu Kh, Isaev E I, Godoniuk A V *Zh. Eksp. Teor. Fiz.* **124** 1121 (2003) [*JETP* **97** 1005 (2003)]
105. Mizutani U J *Phys. Condens. Matter* **10** 4609 (1998)
106. Mizutani U *Mater. Sci. Eng. A* **294 – 296** 464 (2000)
107. Mizutani U, Takeuchi T, Sato H *J. Phys. Condens. Matter* **14** R767 (2002)
108. Bancel P A, Heiney P A *Phys. Rev. B* **33** 7917 (1986)
109. Friedel J *Helv. Phys. Acta* **61** 538 (1988)
110. Smith A P, Ashcroft N W *Phys. Rev. Lett.* **59** 1365 (1987)
111. Vaks V G, Kamyshenko V V, Samolyuk G D *Phys. Lett. A* **132** 131 (1988)
112. Fradkin M A *Pis'ma Zh. Eksp. Teor. Fiz.* **49** 612 (1989) [*JETP Lett.* **49** 705 (1989)]
113. Davydov D N et al. *Phys. Rev. Lett.* **77** 3173 (1996)
114. Widmer R et al. *Philos. Mag.* **86** 781 (2006)
115. Okada J T et al. *J. Phys. Soc. Jpn.* **76** 033707 (2007)
116. Dolinšek J et al. *Phys. Rev. B* **62** 8862 (2000)
117. Kalugin P A, Kitaev A Yu, Levitov L S *Zh. Eksp. Teor. Fiz.* **91** 692 (1986) [*Sov. Phys. JETP* **64** 410 (1986)]
118. Vekilov Yu Kh, Isaev E I *Pis'ma Zh. Eksp. Teor. Fiz.* **75** 703 (2002) [*JETP Lett.* **75** 583 (2003)]
119. Lu J P, Odagaki T, Birman J L *Phys. Rev. B* **33** 4809 (1986)
120. Kalugin P A et al. *Phys. Rev. B* **53** 14145 (1996)
121. Los J, Janssen T, Gahler F *J. Physique I* **3** 1431 (1993)
122. Goldman A I et al. *Phys. Rev. B* **43** 8763 (1991)
123. Goldman A I et al. *Phys. Rev. B* **45** 10280 (1992)
124. Quilichini M et al. *J. Physique I* **51** 1785 (1990)
125. Quilichini M et al. *J. Physique II* **2** 125 (1992)
126. de Boissieu M et al. *J. Phys. Condens. Matter* **5** 4945 (1993)
127. Boudard M et al. *J. Phys. Condens. Matter* **7** 7299 (1995)
128. Quilichini M *Rev. Mod. Phys.* **69** 277 (1997)
129. Shibata K et al. *J. Phys. Condens. Matter* **14** 1847 (2002)
130. de Boissieu M et al. *Nature Mater.* **6** 977 (2007)
131. Dugain F et al., in *Aperiodic'97*: *Proc. of the Intern. Conf. on Aperiodic Crystals, 1997, France* (Eds M de Boissieu, J-L Verger-Gaugry, R Currat) (Singapore: World Scientific, 1997) p. 651
132. Suck J-B *J. Non-Cryst. Solids* **153 – 154** 573 (1993)
133. Dugain F et al. *Eur. Phys. J. B* **7** 513 (1999)
134. Chernikov M A et al. *Phys. Rev. Lett.* **80** 321 (1998)
135. Chernikov M A *Usp. Fiz. Nauk* **175** 437 (2005) [*Phys. Usp.* **48** 411 (2005)]
136. Hafner J, Krajčí M, Mihalkovič M *Phys. Rev. Lett.* **76** 2738 (1996)
137. Poon S J *Adv. Phys.* **41** 303 (1992)
138. Rodmar M et al. *Phys. Rev. B* **60** 10807 (1999)
139. Rapp Ö, in *Physical Properties of Quasicrystals* (Ed. Z M Stadnik) (Berlin: Springer, 1999) p. 127
140. Rapp Ö, Srinivas V, Poon S J *Phys. Rev. B* **71** 012202 (2005)
141. Mooij J H *Phys. Status Solidi A* **17** 521 (1973)
142. Chernikov M A, Isaev E I, Vekilov Yu Kh *Phys. Lett. A* **373** 2179 (2009)
143. Gantmakher V F *Usp. Fiz. Nauk* **172** 1283 (2002) [*Phys. Usp.* **45** 1165 (2002)]
144. Gantmakher V F *Elektrony v Neuporyadochennykh Sredakh* (Electrons and Disorder in Solids) (Moscow: FIZMATLIT, 2005) [Translated into English (Oxford: Clarendon Press, 2005)]
145. Janot C *Int. J. Mod. Phys. B* **8** 2245 (1994)
146. Burkov S E, Timusk T, Ashcroft N W *J. Phys. Condens. Matter* **4** 9447 (1992)
147. Burkov S E, Varlamov A A, Livanov D V *Pis'ma Zh. Eksp. Teor. Fiz.* **62** 361 (1995) [*JETP Lett.* **62** 338 (1995)]
148. Burkov S E, Varlamov A A, Livanov D V *Phys. Rev. B* **53** 11504 (1996)
149. Vekilov Yu Kh, Isaev E I, Livanov D V *Zh. Eksp. Teor. Fiz.* **121** 203 (2002) [*JETP* **94** 172 (2002)]
150. Vekilov Yu Kh, Isaev E I, Johansson B *Phys. Lett. A* **352** 524 (2006)
151. Vekilov Yu Kh, Isaev E I, Johansson B *Solid State Commun.* **133** 473 (2005)
152. Klein T et al. *Europhys. Lett.* **13** 129 (1990)
153. Biggs B D, Poon S J, Munirathnam N R *Phys. Rev. Lett.* **65** 2700 (1990)
154. Lindqvist P et al. *Phys. Rev. B* **48** 630 (1993)
155. Pierce F S, Guo Q, Poon S J *Phys. Rev. Lett.* **73** 2220 (1994)
156. Chernikov M A et al. *Phys. Rev. B* **62** 262 (2000)
157. Kirihara K, Nagata T, Kimura K *J. Alloys Comp.* **342** 469 (2002)
158. Kirihara K, Kimura K *J. Appl. Phys.* **92** 979 (2002)
159. Giannò K et al. *Mater. Sci. Eng. A* **294 – 296** 715 (2000)
160. Homes C C et al. *Phys. Rev. Lett.* **67** 2694 (1991)
161. Degiorgi L et al. *Solid State Commun.* **87** 721 (1993)
162. Basov D N et al. *Phys. Rev. Lett.* **73** 1865 (1994)
163. Burkov S E, Rashkeev S N *Solid State Commun.* **92** 525 (1994)
164. Bianchi A D et al. *Phys. Rev. B* **55** 5730 (1997)
165. Basov D N et al. *Phys. Rev. Lett.* **72** 1937 (1994)
166. Bianchi A D et al. *Phys. Rev. B* **58** 3046 (1998)
167. Ziman J M *Electrons and Phonons* (Oxford: Clarendon Press, 1960) [Translated into Russian (Moscow: IL, 1962)]
168. Wong K M et al. *Phys. Rev. B* **35** 2494 (1987)
169. Graebner J E, Chen H S *Phys. Rev. Lett.* **58** 1945 (1987)
170. Graebner J E et al. *Phys. Rev. Lett.* **39** 1480 (1977)
171. Stadnik Z M et al. *J. Phys. Condens. Matter* **14** 6883 (2002)
172. Azhazha V et al. *Phys. Lett. A* **303** 87 (2002)
173. Azhazha V M et al. *Fiz. Nizkikh Temp.* **31** 629 (2005) [*Low Temp. Phys.* **31** 477 (2005)]
174. Karkut M G, Hake R R *Phys. Rev. B* **28** 1396 (1983)
175. Matsuo S et al. *J. Phys. Condens. Matter* **1** 6893 (1989)
176. Saito K, Matsuo S, Ishimasa T *J. Phys. Soc. Jpn.* **62** 604 (1993)
177. Lück R, Kek S *J. Non-Cryst. Solids* **153 – 154** 329 (1993)
178. Chernikov M A et al. *Phys. Rev. B* **48** 3058 (1993)
179. Hattori Y et al. *J. Phys. Condens. Matter* **7** 2313 (1995)
180. Fisher I R et al. *Phys. Rev. B* **59** 308 (1999)
181. Yokoyama Y, Inoue A, Masumoto T *Mater. Trans. JIM* **33** 1012 (1992)
182. Yokoyama Y et al. *Jpn. J. Appl. Phys.* **33** 3488 (1994)
183. Lin C R et al. *Phys. Lett. A* **196** 365 (1995)
184. Lyubutin I S, Lin Ch R, Lin S T *Zh. Eksp. Teor. Fiz.* **111** 1449 (1997) [*JETP* **84** 800 (1997)]
185. Matsuo S et al. *J. Phys. F* **18** L175 (1988)
186. Krajčí M, Hafner J *Phys. Rev. B* **78** 224207 (2008)
187. Rau D et al. *Eur. Phys. J. B* **46** 281 (2005)
188. Prejean J J et al. *Phys. Rev. B* **73** 214205 (2006)
189. Hippert F et al. *Phys. Rev. B* **68** 134402 (2003)
190. Lasjaunias J C et al. *Phys. Rev. B* **52** 886 (1995)
191. Canella V, in *Amorphous Magnetism* (Eds H O Hooper, A M de Graaf) (New York: Plenum Press, 1973)
192. Ford P J, Mydosh J A *Phys. Rev. B* **14** 2057 (1976)
193. Satoh M et al. *Mater. Sci. Eng. A* **181 – 182** 801 (1994)
194. Chernikov M A et al. *Phys. Rev. B* **68** 094202 (2003)
195. Rau D et al. *Phys. Rev. B* **68** 134204 (2003)
196. Sebastian S E et al. *Philos. Mag.* **84** 1029 (2004)
197. Baberschke K et al. *Phys. Rev. B* **29** 4999 (1984)
198. Sato T J et al. *Phys. Rev. B* **61** 476 (2000)
199. Dolinšek J et al. *Phys. Rev. B* **64** 224209 (2001)
200. Lifshitz R *Phys. Rev. Lett.* **80** 2717 (1998)
201. Charrier B, Schmitt D *J. Magn. Magn. Mater.* **171** 106 (1997)
202. Charrier B, Ouladdiaf B, Schmitt D *Phys. Rev. Lett.* **78** 4637 (1997)
203. Islam Z et al. *Phys. Rev. B* **57** R11047 (1998)
204. Vekilov Yu Kh et al. *Zh. Eksp. Teor. Fiz.* **127** 1279 (2005) [*JETP* **100** 1127 (2005)]
205. Peierls R *Ann. Physik* **395** 1055 (1929)

206. Berman R *Thermal Conduction in Solids* (Oxford: Claredon Press, 1976)
207. Berman R, Brock J C F *Proc. R. Soc. London A* **289** 46 (1965)
208. Freeman J J , Anderson A C *Phys. Rev. B* **34** 5684 (1986)
209. Anderson P W, Halperin B I, Varma C M *Philos. Mag.* **25** 1 (1972)
210. Phillips W A *J. Low Temp. Phys.* **7** 351 (1972)
211. Zaitlin M P, Anderson A C *Phys. Rev. B* **12** 4475 (1975)
212. Cahill D G, Pohl R *Solid State Commun.* **70** 927 (1989)
213. Chernikov M A, Bianchi A, Ott H R *Phys. Rev. B* **51** 153 (1995)
214. Chernikov M A et al., in *Quasicrystals: Proc. of the 5th Intern. Conf., 1995, France* (Eds C Janot, R Mosseri) (Singapore: World Scientific, 1995) p. 569
215. Chernikov M A et al. *Europhys. Lett.* **35** 431 (1996)
216. Vernier N et al. *Europhys. Lett.* **22** 187 (1993)
217. Piche L et al. *Phys. Rev. Lett.* **32** 1426 (1974)
218. Kuo Y K et al. *Phys. Rev. B* **72** 054202 (2005)
219. Edagawa K et al. *Phys. Rev. Lett.* **77** 1071 (1996)
220. Perrot A et al., in *Quasicrystals: Proc. of the 5th Intern. Conf., 1995, France* (Eds C Janot, R Mosseri) (Singapore: World Scientific, 1995) p. 588
221. Huttunen-Saarivirta E *J. Alloys Comp.* **363** 154 (2004)
222. Liu P, Hultin Stigenberg A, Nilsson J-O *Scripta Metall. Mater.* **31** 249 (1994)
223. Nilsson J-O, Liu P, Dzugutov M, in *Quasicrystals: Symp., 30 November-2 December 1998, Boston, MA* (Eds J-M Dubois et al.) (Warrendale, PA: Materials Research Society, 1999) p. 513
224. Inoue A et al., in *Proc. of the 6th Intern. Conf. on Quasicrystals, 26 – 30 May 1997, Tokyo, Japan* (Eds S Takeuchi, T Fujiwara) (Singapore: World Scientific, 1997) p. 723
225. Steurer W, Sutter-Widmer D *J. Phys. D* **40** R229 (2007)
226. Kaputkina N E et al. *Philos. Mag.* **88** 2253 (2008)
227. Zeng X et al. *Nature* **98** 157 (2004)
228. Bindi L et al. *Science* **324** 1306 (2009)